Clim. Past Discuss., 8, 4513–4564, 2012
www.clim-past-discuss.net/8/4513/2012/
doi:10.5194/cpd-8-4513-2012

Climate of the Past Discussions

Modulation of Late Cretaceous and Cenozoic climate by variable drawdown of atmospheric pCO_2 from weathering of basaltic provinces on continents drifting through the equatorial humid belt

D. V. Kent[1,2] **and G. Muttoni**[3,4]

[1]Earth and Planetary Sciences, Rutgers University, Piscataway, NJ 08854, USA
[2]Lamont-Doherty Earth Observatory of Columbia University, Palisades, NY 10964, USA
[3]Department of Earth Sciences, University of Milan, via Mangiagalli 34, 20133 Milan, Italy
[4]ALP – Alpine Laboratory of Paleomagnetism, via Madonna dei Boschi 76, 12016 Peveragno, CN, Italy

Received: 23 August 2012 – Accepted: 28 August 2012 – Published: 13 September 2012

Correspondence to: D. V. Kent (dvk@rutgers.edu)

Published by Copernicus Publications on behalf of the European Geosciences Union.

Abstract

The small reservoir of carbon dioxide in the atmosphere (pCO_2) that modulates climate through the greenhouse effect reflects a delicate balance between large fluxes of sources and sinks. The major long-term source of CO_2 is global outgassing from sea-floor spreading, subduction, hotspot activity, and metamorphism; the ultimate sink is through weathering of continental silicates and deposition of carbonates. Most carbon cycle models are driven by changes in the source flux scaled to variable rates of ocean floor production. However, ocean floor production may not be distinguishable from being steady since 180 Ma. We evaluate potential changes in sources and sinks of CO_2 for the past 120 Ma in a paleogeographic context. Our new calculations show that although decarbonation of pelagic sediments in Tethyan subduction likely contributed to generally high pCO_2 levels from the Late Cretaceous until the Early Eocene, shutdown of Tethyan subduction with collision of India and Asia at the Early Eocene Climate Optimum at around 50 Ma was inadequate to account for the large and prolonged decrease in pCO_2 that eventually allowed the growth of significant Antarctic ice sheets by around 34 Ma. Instead, variation in area of continental basaltic provinces in the equatorial humid belt (5° S–5° N) seems to be the dominant control on how much CO_2 is retained in the atmosphere via the silicate weathering feedback. The arrival of the highly weatherable Deccan Traps in the equatorial humid belt at around 50 Ma was decisive in initiating the long-term slide to lower atmospheric pCO_2, which was pushed further down by the emplacement of the 30 Ma Ethiopian Traps near the equator and the southerly tectonic extrusion of SE Asia, an arc terrane that presently is estimated to account for 1/4 of CO_2 consumption from all basaltic provinces that account for ~ 1/3 of the total CO_2 consumption by continental silicate weathering (Dessert et al., 2003). A negative climate-feedback mechanism that (usually) inhibits the complete collapse of atmospheric pCO_2 is the accelerating formation of thick cation-deficient soils that retard chemical weathering of the underlying bedrock. Nevertheless, equatorial climate seems to be relatively insensitive to pCO_2 greenhouse forcing and thus with availability

of some rejuvenating relief as in arc terranes or thick basaltic provinces, silicate weathering in this venue is not subject to a strong negative feedback, providing an avenue for sporadic ice ages. The safety valve that prevents excessive atmospheric pCO_2 levels is the triggering of silicate weathering of continental areas and basaltic provinces in the temperate humid belt. Increase in Mg/Ca ratio of seawater over the Cenozoic may be due to weathering input from continental basaltic provinces.

1 Introduction

Deep water temperatures determined from the continuous benthic oxygen isotope record (Cramer et al., 2009, 2011; Miller et al., 2005b; Zachos et al., 2001) (Fig. 1a) document that global climate over the past 120 Myr experienced extremes ranging from equable polar climates with bottom water temperatures over 15 °C during the Cretaceous Thermal Maximum (CTM ~ 90 Ma; Wilson et al., 2002) and the Early Eocene Climatic Optimum (EECO, ~ 50 Ma) to a cooling trend during the Middle and Late Eocene with a major sea level fall (Fig. 1b) at around the Eocene–Oligocene boundary (~ 34 Ma), marking the inception of major polar (Antarctic) ice sheets.

The equable conditions at the CTM and especially the EECO are associated with warmer global (polar and tropical) sea surface temperatures (Pearson et al., 2001, 2007) that most likely resulted from an enhanced greenhouse effect due to higher atmospheric pCO_2 concentrations as inferred from various proxies (Fig. 1c; see review with references in Beerling and Royer, 2011; Royer, 2010). These high pCO_2 levels have been conventionally attributed to higher rates of ocean crust production and associated increased outgassing (Berner et al., 1983), for example, a presumed pulse of increased global sea-floor spreading and the emplacement of the North Atlantic igneous province at the EECO (Miller et al., 2005a; Rea et al., 1990; Thomas and Bralower, 2005; Zachos et al., 2001). Decreasing pCO_2 levels (Pagani et al., 2005, 2011) and the seemingly coincident cooling trend that followed the EECO could then be due to reduced outgassing flux from lower global ocean floor production rates and eventually

led to a major buildup of Antarctic ice sheets at around the Eocene–Oligocene boundary (DeConto and Pollard, 2003), whose precise evolution may have been influenced by openings of Southern Ocean gateways (Kennett, 1977; Livermore et al., 2007; Stickley et al., 2004).

A spreading rate-dependent outgassing factor (Berner, 1994; Berner et al., 1983; Engebretson et al., 1992) is intuitively appealing and widely regarded as the most important parameter driving variations in pCO_2 in the current generation of carbon cycling models (Berner, 2004) but there are conflicting estimates of global ocean floor production rates. For example, Muller et al. (2008) and Seton et al. (2009) postulate high production in the Late Cretaceous and decreasing production in the Cenozoic whereas Cogné and Humler (2004, 2006) show high production earlier in the Cretaceous, reduced production in the later Cretaceous, and increasing production over the Cenozoic. Provocatively, Rowley (2002) showed that the observed area-age versus age distribution of oceanic crust does not require substantial production rate changes since the breakup of Pangea at 180 Ma; the fact that more than 50 % of oceanic lithosphere younger than 55.7 Ma (70 % younger than ~ 89 Ma, 85 % younger than ~ 120 Ma) has already been removed by subduction means that reconstructions of oceanic lithosphere history are invariably based on substantial and often poorly constrained extrapolations (Rowley, 2008). Moreover, carbon-uptake by oceanic crust may tend to cancel any residual spreading rate-dependent variations in CO_2 outgassing (Berner, 1990a,b; Brady and Gislason, 1997; Staudigel et al., 1989, 1990a,b). Increased CO_2 flux from mantle plumes most likely occurred during the relatively short emplacement times of individual LIPs but the time-integrated effect may not be very important on the million year time scale (Marty and Tolstikhin, 1998), an assessment supported by new proxy measurements of pCO_2 that support models (e.g., Caldeira and Rampino, 1990; Dessert et al., 2001) showing that increases associated with a major LIP emplacement decay away on less than a million year time scale (Schaller et al., 2011).

The generally high pCO_2 levels and warm polar climates that characterized the mid-Cretaceous to Early Eocene may have had a substantial contribution from the

protracted subduction of Tethyan pelagic carbonates deposited on the Indian plate during northward drift from ~ 120 Ma until collision of Greater India with Asia (Lhasa block) at ~ 50 Ma (Edmond and Huh, 2003; Hansen et al., 2008; Kent and Muttoni, 2008; Schrag, 2002). The ensuing long-term trend of decreasing pCO_2 levels and temperatures from 50 Ma to the onset of Antarctic glaciation at 34 Ma may thus have resulted from re-equilibration to the reduced CO_2 flux with the shutdown of the Tethyan decarbonation factory. Alternatively, intense weathering of the Deccan Traps as they drifted into the equatorial humid belt may have increased the consumption of CO_2 (Dessert et al., 2003; Kent and Muttoni, 2008).

In this paper, we elaborate on the tectonic forcing of pCO_2 variations using plate tectonic reconstructions in a paleolatitudinal reference frame and attempt to quantify (a) the decarbonation potential of Tethyan subduction since ~ 120 Ma as a potential additional source of CO_2, and (b) the silicate weathering potential for higher consumption of CO_2 of continental areas and especially highly weatherable basaltic provinces as they drifted through the equatorial humid belt, the most potent venue for continental silicate weathering (Dessert et al., 2003). We evaluate the relative contributions of these modes of steering atmospheric pCO_2 as well as other alternative mechanisms, including proposed changes in organic carbon burial inferred from trends in $\delta^{13}C$ carbonate records (Katz et al., 2005) and the uplift-weathering hypothesis (Raymo and Ruddiman, 1992; Raymo et al., 1988). The degree of sensitivity of global climate to changes in atmospheric pCO_2 is difficult to gauge but we mainly seek to explain the generally high pCO_2 levels from the CTM to EECO (~ 90 to 50 Ma) and the decrease to generally low pCO_2 levels that characterize the Oligocene to Present (from ~ 34 Ma). Modeling studies point to threshold decreases in atmospheric pCO_2 as the most likely causes for widespread Antarctic glaciation at around the Eocene–Oligocene boundary (Oi-1, ~ 34 Ma; DeConto and Pollard, 2003; DeConto et al., 2008) and the onset of permanent Northern Hemisphere glaciations in the late Pliocene (~ 3 Ma; Lunt et al., 2008).

2 Paleogeographic reconstructions from 120 Ma to present

In the absence of compelling evidence for long-term secular changes in global ocean floor production and subduction rates, we assume that the background CO_2 outgassing rate held steady and was comparable to the modern outgassing rate of ~ 260 (range of plausible estimates of 180 to 440) Tton CO_2 Myr^{-1} (where Tton = 10^{12} ton = 10^{15} kg, and Myr = 10^6 yr)(Gerlach, 2011; Marty and Tolstikhin, 1998). To estimate contributions of CO_2 outgassing from the subduction of carbonate-rich sediments and consumption of CO_2 from silicate weathering of continental areas as they drifted through different climate zones, we generated paleogeographic reconstructions of the main continents using a composite apparent polar wander path (APWP) (Fig. 2; Table 1) and the finite rotation poles used by Besse and Courtillot (2002) from Muller and Roest (1992), Muller et al. (1993) and Srivastava and Tapscott (1986). The composite APWP uses paleopoles from all the main continents rotated to common coordinates (in this case, North America) and averaged in a sliding 20 Myr window every 10 Myr. The mean paleopole for 60 to 120 Ma is an average of global igneous data from Kent and Irving (2010) for a standstill in APW in North American coordinates; we averaged their 60, 80, 100 and 120 Ma mean poles, which are independent, to derive a 60–120 Ma superpole. Mean paleopoles for 10 to 50 Ma, which are dominated by global igneous data and thus also less prone to be biased by inclination error, are from Besse and Courtillot (2002, 2003). The composite APWP should record the geocentric axial dipole field, hence the different APWP for the various continents shown in Fig. 2 simply reflect their relative motions according to the finite rotation model. Uncertainty in latitudinal positions of the continents should be on the order of the radii of circles of 95 % confidence around the mean paleopoles (~ 3°; Table 1).

The main elements of the plate tectonic scenario are the convergence of Greater India with the Lhasa block, which was accreted to Asia before the Late Jurassic (Allègre et al., 1984; Chang and Cheng, 1973), and the convergence of Arabia with the Iran block, which was accreted to Asia during the Late Triassic–Early Jurassic Cimmerian

orogeny (e.g., Muttoni et al., 2009; Zanchi et al., 2009) and was only moderately disrupted by oblique subduction of the Tethyan Ocean in the Cretaceous (Moghadam et al., 2009). A related tectonic feature is the extrusion of the SE Asian blocks during the indentation of India into Asia (Molnar and Tapponnier, 1975). There is a vast literature on various aspects of the tectonics of the Himalaya and adjacent Tibetan Plateau (e.g., more than 330 cited references in a review paper by Yin and Harrison, 2000 and more than 500 cited references in one by Hatzfeld and Molnar, 2010), but what is critical to our analysis is to locate within these reconstructions the position of the Asian margin (Lhasa, Iran) and of the SE Asian blocks, which was done as follows.

1. The southern (collisional) margin of the Lhasa block was drawn assuming that it coincided in shape and location with the northern margin of Greater India (which is much easier to place using the APWP described above) at full India-Lhasa collision at 50 Ma; for pre-50 Ma times, the Lhasa margin was kept coherent and therefore rotated with Asia. The ~ 50 Ma collision age, instrumental to locate the position of the margin, is based on several lines of geological evidence (Garzanti, 2008; Garzanti et al., 1987; Zhu et al., 2005; and references therein), and is supported by the marked decrease in convergence rate between India and Eurasia observed in the Indian Ocean between magnetic Anomaly 22 (~ 49.5 Ma) and Anomaly 21 (~ 48.5 Ma) (Copley et al., 2010; Patriat and Achache, 1984; see also Cande and Stegman, 2011; Molnar and Stock, 2009). An age of ~ 50 Ma for the India-Lhasa collision is preferred to the much younger age of ~ 35 Ma envisaged by Aitchison et al. (2007) and Ali and Aitchison (2008) essentially for the arguments made by Garzanti (2008). Our reconstructions are in substantial agreement with the available albeit sparse paleomagnetic data indicating that the margin had a paleolatitude comprised between ~ 10° N and ~ 20° N in the Cretaceous-Early Cenozoic (Achache et al., 1984; Chen et al., 1993, 2012). Other results and compilations of paleomagnetic data that try to take into account sedimentary flattening of paleomagnetic directions suggest that collision with Northern India occurred at 46 ± 8 Ma (Dupont-Nivet et al., 2010) and that the southern margin

of the Lhasa block extended as far south as 20° N during the Eocene (Lippert et al., 2011), which we regard as in substantial agreement with our reconstructed tectonic framework given the uncertainties in reference paleopoles.

2. Following similar reasoning, the southern (collisional) margin of the Iran block was drawn assuming that it coincided with the northern margin of Arabia at full collision at ~ 20 Ma. The Arabia–Iran collision may have started at ~ 35 Ma based on geologic evidence (Agard et al., 2005; Allen and Armstrong, 2008); however, complete Western Tethys closure seems not to have occurred until ~ 20 Ma based on recent apatite fission-track data indicating that the last oceanic lithosphere between Arabia and Eurasia was not consumed until the Early Miocene (Okay et al., 2010).

3. The position of the SE Asia blocks (North, Central, and South Indochina, West and East Sumatra, Borneo, and Java) have been reconstructed in the 0–40 Ma interval using the (cumulative) rotation poles of Replumaz and Tapponnier (2003) relative to Siberia (Eurasia) (Table 2). For the previous 50–120 Ma interval, the SE Asia blocks are considered tectonically coherent and moved with Siberia (Eurasia). Accordingly, our Cretaceous reconstructions are similar to those of Chen et al. (1993) with Indochina placed using Cretaceous paleomagnetic data from Yang and Besse (1993) across paleolatitudes spanning from ~ 10° N to 30° N close to Siberia. Moreover, our 65 Ma reconstruction predicts a paleolatitude for western Yunnan (North Indochina block) that is consistent, within paleomagnetic resolution, with a paleolatitude of 17° ± 9° N calculated for the area from (sparse) paleomagnetic data from the Paleocene (Yang et al., 2001). Southward extrusion of the SE Asia blocks basically stopped at about 15 Ma with cessation of seafloor spreading in the South China Sea (Briais et al., 1993) even though overall southerly movement continued as Eurasia rotated clockwise according to its APWP. Our reconstructions are similar to the classic India-SE Asia indentor-extrusion model (Molnar and Tapponnier, 1975; Replumaz and

Tapponnier, 2003; Royden et al., 2008) and differ from alternative reconstructions that question evidence for extrusion and locate the SE Asia blocks since before the onset of India-Asia collision at essentially the latitudes they are found today (Aitchison et al., 2007; Hall et al., 2008; see also exchange between Garzanti, 2008, and Aitchison et al., 2008). Hall et al. (2008) support their fixist reconstructions citing paleomagnetic data from Borneo and surrounding regions (Fuller et al., 1999; Schmidtke et al., 1990) that (a) do not seem to indicate a clear pattern of clockwise rotations, and (b) show no consistent southward displacement of blocks over the Cenozoic, both expected from the extrusion model. As acknowledged by Fuller et al. (1999), however, the quality of the paleomagnetic data from Borneo is problematical given that many results come from igneous intrusions with no control on paleohorizontal and "the intimate mixing throughout Borneo of rotated and unrotated results is easier to explain in terms of remagnetization than by a special distribution of local shears". The details of the paleolatitudinal evolution of Borneo can hardly be resolved by these data. However, results from the late Cretaceous and early Cenozoic Segamat basalts and supporting data from the Kuantan dike swarm all from the Malaysia Peninsula indicate paleolatitudes at time of emplacement of 20° N (compared to a present-day latitude of ∼ 2.5° N) (Richter et al., 1999) and provide in our opinion robust (e.g., not influenced by sedimentary inclination flattening) paleomagnetic data in support of the SE Asia southward extrusion model and Eurasia clockwise rotation.

Greater India resided for much of the Mesozoic in the Southern Hemisphere as part of the classical Gondwana supercontinental assembly (Smith and Hallam, 1970), which began to disperse in the Late Jurassic with the opening of the Somali basin (Rabinowitz et al., 1983) and the separation of East Gondwana (which included India, Madagascar, Antarctica, and Australia) from West Gondwana (Africa and South America). Greater India commenced its ∼ 6000 km northward drift toward Lhasa (Asia) when it separated (with Madagascar) from Antarctica at around 120 Ma (Fig. 3a) and continued its journey after separation from Madagascar at around 84 Ma, approached the equatorial belt

(5° S–5° N) at 65 Ma (Fig. 3b) and began to collide with Asia at around 50 Ma (Fig. 3c). The extrusion of the SE Asian blocks with the indentation of India into Asia was such that at ∼ 30 Ma Borneo was approaching the equatorial humid belt (Fig. 3d). Convergence between Arabia–Iran caused final collision at ∼ 20 Ma, whereas the southward extrusion of SE Asia largely ceased by ∼ 15 Ma (Fig. 3e) although continued clockwise rotation of Eurasia gradually brought SE Asia to its present position (Fig. 3f).

3 Did the Tethyan CO_2 factory produce Cretaceous–Eocene greenhouse climate?

The northward drift of India involved the subduction under Asia of oceanic crust that must have transited through the equatorial belt (Fig. 3a–c). This is because the paleomagnetic (i.e., latitudinal) constraints indicate that the Lhasa (Asia) southern margin remained in the Northern Hemisphere (10° N–20° N) from practically the time India separated from Antarctica at ∼ 120 Ma until incipient collision at ∼ 50 Ma. In modern oceans, equatorial regions are generally associated with upwelling and high organic productivity, giving rise to enhanced deposition of biogenic sediments (Berger and Winterer, 1974) that sequester CO_2 from the atmosphere. This has been especially true since the diversification of planktonic marine protists by the mid-Mesozoic, when open oceans became important loci of carbonate deposition, progressively replacing shallow water carbonates (Wilkinson and Walker, 1989). Calcareous nannoplankton became the most efficient sediment-forming group in Cretaceous oceans, sometimes forming thick chalk deposits, whereas planktonic foraminifers became relevant sediment-producers only since the Late Cretaceous (Erba, 2004). Biogenic sediments deposited on oceanic crust are more readily subducted than shallow water carbonates on buoyant continental crust, hence pelagic sediments are more prone to metamorphic decarbonation, potentially augmenting the global flux of CO_2 to the atmosphere (Caldeira, 1992; Volk, 1989). The subduction of Tethyan sea floor from 120 Ma to 50 Ma may thus have constituted a productive source of additional CO_2, which according to some scenarios may have

been responsible for the generally equable climates in the Cretaceous to Eocene (Edmond and Huh, 2003; Hansen et al., 2008; Kent and Muttoni, 2008; Schrag, 2002). Alternatively, much of the subducted carbon may have remained buried in a deep-seated mantle reservoir (Selverstone and Gutzler, 1993). Here we attempt to estimate the maximum amount of subducted carbon as a source of CO_2 to the atmosphere by invoking high biogenic productivity on oceanic crust and assuming that an appreciable fraction of the subducted carbon is returned to the atmosphere.

We estimated the productivity of the Tethyan CO_2 factory over the Cretaceous–Cenozoic by reconstructing the latitudinal component of motion for a point on the northern margin of the Indian plate (filled star in Fig. 3a) compared with the latitudinal evolution of a point on the Lhasa southern margin (unfilled star in Fig. 3a). The paleolatitude curves (Fig. 4a) were used to predict the timing of subduction of oceanic crust attached to Greater India that was loaded with equatorial (5° S–5° N) bulge sediments. In a simple 2-plate model, the onset of northward motion of Greater India at ~ 120 Ma presaged the onset of subduction of the equatorial bulge underneath the Lhasa margin at around 97 Ma and until the bulge that formed under the equatorial belt at around 72 Ma was subducted at ~ 55 Ma and the last sediments were consumed in the trench at 50 Ma. In other words, a full equatorial load of sediment was probably continuously subducted in southern Asia trenches from at least ~ 97 Ma to collision at 50 Ma.

The amount of equatorial bulge sediments subducted with time can be estimated from the loading time, loading area, and mass accumulation rate, as follows:

1. The time spent by the Tethyan crust under the presumed 5° S–5° N upwelling belt (loading time) was calculated acknowledging that the Tethyan crust was loading sediments under the 5° S–5° N belt since well before the onset of India–Asia convergence; we therefore assumed an initial, nominal loading duration of 20 Myr to which we added the loading times directly derived from the plate's latitudinal velocity (Fig. 4b). For example, oceanic crust entering the Lhasa trench at ~ 80 Ma (Fig. 4a) was already sediment-loaded for 20 Myr when it started moving from

5° S at 120 Ma across the equatorial belt to 5° N at 89 Ma thus accumulating additional ~ 31 Myr of loading (total of ~ 51 Myr at subduction; Fig. 4b). As another example, oceanic crust entering the Lhasa trench at ~ 70 Ma (Fig. 4a) was already sediment-laden for 20 Myr when it crossed the equatorial belt from ~ 93 Ma to ~ 78 Ma accumulating an additional ~ 16 Myr of loading (total of ~ 36 Myr at subduction; Fig. 4b).

2. The surface area of Indian oceanic crust displaced northward at any given time and eventually consumed at the trench (subduction rate) was calculated from the paleogeographic reconstructions (Fig. 3 and additional ones) and found to steadily increase from ~ 0.09 $Mkm^2\,Myr^{-1}$ to ~ 0.45 $Mkm^2\,Myr^{-1}$ for a total subducted crust of ~ 19.0 Mkm^2 (Fig. 4d). Most of this crust (~ 14.7 Mkm^2) resided on or crossed the equatorial upwelling belt before being subducted, whereas the remainder (~ 4.3 Mkm^2) was located between 5° N and the Lhasa margin and presumably never got loaded with equatorial sediments (see Fig. 3a).

3. A nominal mass accumulation rate (MAR) of 1.5 $g\,cm^{-2}\,kyr^{-1}$ (15 $Mton\,km^{-2}\,Myr^{-1}$) for the Tethyan equatorial belt 5° S–5° N was derived from estimates for the Cretaceous equatorial Pacific Ocean (Ogg et al., 1992), which is within the range of values found for the Cenozoic equatorial Pacific (Mitchell and Lyle, 2005; Mitchell et al., 2003).

Summarizing and clarifying the above, oceanic crust transiting under the equatorial upwelling belt gets a full biogenic (calcareous and biosiliceous) sediment load that is estimated by multiplying the loaded time (1) by the loading area (2) by the MAR value (3). This subducted load is found to vary between ~ 60 $Tton\,Myr^{-1}$ at ~ 120 Ma up to ~ 220 $Tton\,Myr^{-1}$ at ~ 80 Ma and dropping to virtually zero at 50 Ma (Fig. 4d). Even allowing the subducted sediment to be entirely carbonate, a recycling rate of 10 % (although generally less) based on ^{10}Be data in arc volcanics (Tera et al., 1986) would imply that the amount of CO_2 that was potentially generated by the decarbonation of Tethyan pelagic biogenic sediments was maximally ~ 9.7 Tton $CO_2\,Myr^{-1}$ at around

80 Ma, corresponding to only ∼ 4 % of the modern outgassing rate of ∼ 260 Tton CO_2 Myr^{-1} (Fig. 4d).

A similar scenario of convergence and equatorial bulge subduction can be traced between Arabia and Iran in the Western Tethys (Fig. 4e–h). Using the procedure outlined above for India, the mean latitudinal velocity of a point on northeastern margin of Arabia (filled circle in Fig. 3a) is used in conjunction with the paleolatitude evolution of a point on the Southwestern Iran margin (unfilled circle in Fig. 3a) to predict that the oceanic crust loaded with equatorial bulge sediments started subducting at around 74 Ma and ended at ∼ 20 Ma with the terminal Arabia–Iran collision (Fig. 4e). The loading time of this subducted oceanic crust was estimated to steadily increase from an initial value of ∼ 20 Myr (for similar reasons previously illustrated for India) to a maximum of ∼ 60 Myr (Fig. 4f). The subduction rate was found to decrease from ∼ 0.18 Mkm^2 Myr^{-1} to ∼ 0.04 Mkm^2 Myr^{-1} for a total subducted crust of ∼ 8.1 Mkm^2 (Fig. 4g). Of this crust, only ∼ 2.1 Mkm^2 resided on or crossed the equatorial upwelling belt before being subducted, whereas the remainder presumably never got loaded with equatorial sediments (see Fig. 3a). These numbers lead us to calculate a subducted sediment load that varies between ∼ 23 Tton Myr^{-1} at 70 Ma and ∼ 35 Tton Myr^{-1} at 20 Ma (Fig. 4h); assuming again that the subducted sediments were entirely carbonates and a recycling rate of ∼ 10 %, the maximum amount of CO_2 that was potentially generated by the decarbonation of these biogenic sediments was ∼ 1.6 Tton CO_2 Myr^{-1} at around 20 Ma, corresponding to only ∼ 0.6 % of the modern outgassing rate of ∼ 260 Tton CO_2 Myr^{-1} (Fig. 4h).

It appears that subduction decarbonation of Tethyan pelagic sediments may have reached ∼ 10 Tton CO_2 Myr^{-1} from 80 to 50 Ma, which is only ∼ 4 % of the modern outgassing rate of 260 Tton CO_2 Myr^{-1}. We can also approach this from the long-term mean ocean production rate of 3.4 Mkm^2 Myr^{-1} from Rowley (2002), which would imply that 340 Mkm^2 of oceanic crust was subducted globally in the 100 Myr from 120 Ma (about when pelagic carbonates and chalks become important) to 20 Ma (end of major Tethyan subduction after which there has been only minor overall subduction of pelagic

carbonates elsewhere, mainly Central America), or nearly 13-fold what was calculated for subduction just of Tethyan crust (∼ 27 Mkm^2 for India plus Arabia). However, a substantial fraction of the oceanic crust that was subducted must have been in the Pacific which did not systematically transit through the equatorial upwelling belt and consequently probably had a much lower MAR, perhaps by an order of magnitude (∼ 1.5 Mton km^{-2} Myr^{-1}) than for equatorial bulge pelagic sedimentation (Mitchell and Lyle, 2005). Even if additional subduction decarbonation doubled the rate estimated just for Tethyan pelagic sediments, to perhaps 20 Tton CO_2 Myr^{-1}, this would nevertheless still be a small fraction (less than 10 %) of the modern CO_2 outgassing rate. This leads us to conclude that unless its efficiency was much higher (Johnston et al., 2011) the decarbonation subduction factory was a rather small contributing factor in producing higher pCO_2 and presumably related warm climate in the Cretaceous–Eocene. We also note that the total deep (mantle) carbon storage of about 1000 Tton CO_2 for the past 125 Myr suggested by Selverstone and Gutzler (1993) to be in response to the Alpine–Himalaya collision amounts to about the same magnitude flux (8 Tton CO_2 Myr^{-1}) as the decarbonation flux and would thus further reduce its relative importance as a net long-term source of CO_2. More generally, subduction decarbonation would seem to be precluded as a major source of CO_2 prior to when open oceans became important loci of carbonate deposition with the abundant appearance of calcareous plankton at ∼ 120 Ma. Edmond and Huh (2003) reached similar conclusions about the general efficacy of subduction decarbonation as a source of CO_2.

Mantle CO_2 that emanated from the emplacement of submarine LIPs (e.g., Ontong Java Plateau, South Kerguelen Plateau, Caribbean Plateau and the North Atlantic Igneous Province) probably significantly increased global pCO_2 levels and triggered various paleoceanographic events (e.g., Tejada et al., 2009) but for not much longer than each of their relatively short emplacement times (Self et al., 2005). This is because model calculations (Dupré et al., 2003; Misumi et al., 2009) and available supporting proxy measurements (Schaller et al., 2011) indicate that the excess CO_2 would be adsorbed by negative feedback mechanisms on less than a million year time scale. In

fact, continental LIPs are likely to be net CO_2 sinks levels due to enhanced consumption from their weathering (Dessert et al., 2003; Schaller et al., 2012).

4 Variable weathering sinks of CO_2

If the long-term source flux of CO_2 stayed basically constant and experienced only transient changes, persistent variations in CO_2 sink fluxes must have been in the driver's seat in controlling the concentration of atmospheric pCO_2. The most important CO_2 sink is weathering of continental silicates (Walker et al., 1981), a negative feedback mechanism dependent on surface temperature and runoff as a function of the CO_2 greenhouse effect and incorporated in most quantitative carbon-cycling models (e.g., Berner, 1991, 1994, 2006; Berner and Kothalava, 2001; Berner et al., 1983).

Recent evaluations have emphasized the importance of continental basalt weathering as a major sink for atmospheric CO_2, representing anywhere from one-third to nearly one-half of the consumption flux from weathering of all continental silicates even though subaerial basalt provinces today constitute less than 5 % of world land area (Table 2 in Dessert et al., 2003). The compilation of Dessert et al. (2003) also shows that for a given gross basin lithology (granitic or basaltic), chemical weathering and CO_2 consumption rates are strongly dependent on runoff and temperature, which are markedly potent in the equatorial humid belt. It is noteworthy that SE Asia in the equatorial humid belt with a mean annual temperature of 25 °C and nearly 140 cm yr^{-1} runoff has by far the highest CO_2 consumption flux (1.033×10^{12} mol yr^{-1} = 45.5 Mton CO_2 yr^{-1}), which constitutes nearly a third of the total CO_2 consumption flux (3.109×10^{12} mol yr^{-1} = 123.8 Mton yr^{-1}) estimated for all basaltic provinces, even though SE Asia represents less than 8 % of the surface area of all continental basalt provinces. In contrast, basalt provinces in cold or dry regions are not weathering rapidly and are thus consuming far less CO_2. For example, the Siberian Traps, a LIP that was emplaced in the latest Permian and presently straddles the Arctic Circle with a mean annual temperature of −10 °C and 40 cm yr^{-1} runoff, contributes a paltry

1.7 % (0.053×10^{12} mol yr^{-1} = 2.3 Mton CO_2 yr^{-1}) to the overall basalt CO_2 consumption flux even though it represents nearly 12 % of the total surface area of continental basalt provinces today (Dessert et al., 2003). The Ethiopian Traps, with a comparable surface area to the Siberian Traps, are just within the tropical arid belt with a much higher mean annual temperature of 21 °C but only 13 cm yr^{-1} runoff and hence end up contributing only 3.9 % (0.121×10^{12} mol yr^{-1} = 5.3 Mton CO_2 yr^{-1}) to the overall basalt CO_2 consumption flux (Dessert et al., 2003). Mg and Ca-poor granitic terranes have CO_2 consumption fluxes that are 2 to 10 times lower than basaltic provinces in comparable climate conditions (Dessert et al., 2001; Gaillardet et al., 1999).

To gauge the latitudinal position of climate belts in the past, we use values for zonal mean annual surface air temperature and the difference between precipitation and evaporation ($P-E$) based on a general circulation model from Manabe and Bryan (1985) with idealized geography, an annual mean insolation, and atmospheric pCO_2 concentrations that vary from one-half to 8-times the modern (pre-industrial: 280 ppm) value. Compared with studies of silicate weathering rate using more comprehensive global climate numerical models (e.g., Donnadieu et al., 2006; Godderis et al., 2008) that include a variety of feedbacks as well as monsoons and other phenomena related to details of geography, the idealized zonal model employed here has the advantage, at this stage, of allowing us to keep the latitudinal dependency of climate fixed while varying the distribution of land masses. Although the amplitude or climate severity of $P-E$ increases with increasing pCO_2, the latitudinal positions of the crossovers ($P-E = 0$) stay relatively fixed (Manabe and Bryan, 1985). Accordingly, we set the equatorial humid belt ($P > E$) as occurring between 5° S and 5° N and the hemispheric limits of the tropical arid belts ($P < E$) as extending from 5° to 30° latitude and that of the temperate humid belts from 30° to the latitudinal limits (60°) of our paleogeographic maps (Fig. 3). Zonal mean temperatures generally increase with higher pCO_2 but for any given pCO_2 level they are uniformly high in the tropics (nominally 23° S to 23° N) before decreasing to about two-thirds of equatorial values by the lower latitude regions of the temperate humid belts (30° N or S) and to around freezing (0 °C) by 60° N or S for

today's pCO_2 level. The most potent and persistent combination of high temperature and high moisture for silicate weathering clearly resides in the equatorial humid belt (5° S–5° N, a zone which constitutes 44 Mkm^2 or 8.7 % of Earth's total surface area) at any pCO_2 level and that is where we focus attention in estimating CO_2 consumption rates.

5 Quantification of CO_2 silicate weathering sinks

Total continental area in the equatorial humid belt was relatively steady at ~ 12 Mkm^2, which is a little more than one-quarter (27 %) of the available surface area in this zone and about 8 % of total continental area (149 Mkm^2), from at least 120 Ma to around 65 Ma (Fig. 5a; see also paleogeography in Fig. 3a,b). Over this time interval, South America had a decreasing areal contribution that was essentially balanced by Africa plus Arabia's increasing areal contribution in the equatorial humid belt. Other land areas had almost negligible contributions until the arrival of Greater India, whose northward passage through the equatorial humid belt provides the distinctive humped signature of the total area curve (Fig. 5a). From the peak of 15 Mkm^2 at ~ 55 Ma, total land area within the equatorial humid belt decreased with the northward indentation of India into Asia and leveled out at around 11 Mkm^2 by 25 Ma when the southerly motion of SE Asia (plus the widening equatorial expanse of South America and the northerly motion of New Guinea attached to Australia) balanced the decreasing contributions from the narrowing equatorial expanse of Africa.

The only large land-based basalt province straddling the equatorial humid belt during the entire Mesozoic was the 201 Ma (earliest Jurassic) Central Atlantic magmatic province (CAMP; Marzoli et al., 1999), whereas the 250 Ma Siberian Traps remained in high (> 50° N) latitudes, the 130 Ma Parana province of South America was in the austral tropical arid belt, and the ~ 120 Ma Rajmajal Traps formed poleward of 50° S in the austral temperate humid belt (Fig. 3). Although CAMP flood basalts were apparently emplaced over a huge area across tropical central Pangea, only scattered dikes and sills with minor exposures of lavas in isolated rift basins now remain (McHone, 2003).

The bulk of the CAMP lavas were probably weathered, eroded or buried soon after their emplacement in the earliest Jurassic. This is compatible with a systematic decrease in atmospheric pCO_2 from paleosols formed within less than a million years of CAMP lavas in eastern North America that is most likely due to consumption via silicate weathering (Schaller et al., 2012). In any case, we suppose that what exposed CAMP fragments remained were probably too small or had already drifted out of the equatorial humid belt to be important factors in weathering consumption by Cretaceous times. The more or less constant area (0.9 Mkm^2) of basaltic rocks from 120 Ma to 50 Ma is mostly in the Andes of South America with some contribution from the Sumatra–Java arc (Fig. 5b).

The Deccan Traps (current surface of 0.5 Mkm^2; original volume of ~ 2 Mkm^3; Courtillot and Renne, 2003) were emplaced at ~ 65 Ma in the austral arid belt (Fig. 3b) and in our view became a major consumer in the long-term CO_2 budget only when the continental LIP that was riding on the India plate drifted into the equatorial humid at 50 Ma (Fig. 3c), just about when Greater India began to collide with Asia. At 30 Ma, the Ethiopian Traps (current surface of 0.4 Mkm^2 = 1/2 of original surface; Rochette et al., 1998) erupted virtually on the equator just as the Deccan Traps drifted out of the equatorial humid belt where Java and Sumatra already began to impinge (Fig. 3d). Tectonic extrusion of SE Asia may have effectively ceased by 15 Ma but a gradual southerly drift due to Eurasia clockwise rotation brought Borneo into the equatorial humid belt (Fig. 3e) where it was eventually joined by New Guinea (attached to Australia) coming from the south (Fig. 3f). Today, there are more than 2 Mkm^2 of highly weatherable basaltic and mixed arc and related rocks in the equatorial humid belt (Fig. 5b).

To estimate the CO_2 consumption rate of the varying land areas within the equatorial humid belt as a function of time, we use the following rates for the dominant lithologies. The rate for basaltic-rich provinces (Deccan and Ethiopian traps, Andes, Java and Sumatra arc) was set to a nominal value of 100 Mton CO_2 Myr^{-1} km^{-2}; this value represents a rounded estimate falling in the lower (conservative) side of a present-day CO_2 consumption span ranging from 84.5 Mton CO_2 Myr^{-1} km^{-2} for SE Asia in toto to

282 Mton CO_2 Myr^{-1} km^{-2} for the island of Java alone (Dessert et al., 2003). A nominal 1/2 of the basalt weathering rate (50 Mton Myr^{-1} km^{-2}) was applied to mixed (basaltic-granitic-gneissic) land areas (South Indochina, Borneo, New Guinea) following Dessert et al. (2001); for example, the basaltic island of Réunion (21° S; ~ 240 cm yr^{-1} runoff, 19 °C mean annual temperature) has an annual CO_2 consumption rate that is roughly twice that of the climatically similar, mixed basaltic-granitic island of Puerto Rico (18° N, ~ 360 cm yr^{-1} runoff, 22 °C mean annual temperature; Fig. 2 in Dessert et al., 2001). CO_2 consumption rates for continental cratonic regions are expected to be much lower due to much less weatherable granitic lithologies (i.e., deficient in Mg and Ca) and generally low topographic relief (i.e., transport-limited regimes; see Sect. 9 below). With all due caveats, we use 5 Mton Myr^{-1} km^{-2} for continental cratonic areas, a rate that is an order of magnitude less than for mixed lithology land areas like New Guinea and compatible with the relative sense of CO_2 consumption rates deduced from the chemistry of large rivers in such areas (Gaillardet et al., 1999).

Paleotemperature estimates from planktonic foraminiferal oxygen isotope records point to tropical climate throughout the Eocene only a few degrees warmer than modern sea-surface temperatures (Pearson et al., 2007). Extrapolation to the past of modern CO_2 consumption rates for the tropics should therefore provide reasonably compatible estimates as far as the temperature component is concerned although the ancient weathering rates are still likely to be underestimated due to more vigorous hydrological cycles during times of higher atmospheric pCO_2 levels.

CO_2 consumption values corresponding to these rates were calculated for areas of subaerial basalts and mixed crust and for the remaining continental cratonic areas in the equatorial humid belt in 5 Myr intervals (Fig. 6). Under these assumptions, areas of subaerial basalts and mixed crust contribute about 50 % more than the remaining much vaster continental cratonic areas (all in the equatorial humid belt) from 120 to 50 Ma, after which the contribution of subaerial basalts and mixed crust eventually increases to nearly 3.5 times that of the remaining continental cratonic areas. The combined CO_2 consumption profile for all subaerial crust in the equatorial humid belt

(top curve in Fig. 6) has much of the character of the potent subaerial basalts and mixed crust component, for example, the downward blip at ~ 35 Ma is essentially due to an apparent gap of highly weatherable basalts in the equatorial humid belt between the northward drift of the Deccan Traps out of the belt before the eruption of the Ethiopian Traps at 30 Ma (Fig. 5b). We cannot exclude that this short-term variation might in part be an artifact associated with uncertainties of a few degrees in paleolatitudes or with phenomena, like monsoons, not taken into account with the simple zonal climate model used to fix the latitudinal bounds of the equatorial humid belt. Hence the smoothed curve in Fig. 6 may provide a more substantiated representation at this juncture of the secular change in total consumption of CO_2. It is remarkable that the estimated CO_2 consumption of up to 190 Tton Myr^{-1} from silicate weathering of only a small fraction of total land with basaltic and mixed crust provinces currently residing in the equatorial humid belt may balance a substantial fraction (> 2/3) of modern total CO_2 outgassing of 260 Tton CO_2 Myr^{-1}.

6 Role of organic carbon burial

Burial of organic carbon can also sequester atmospheric pCO_2. Secular changes of the relative fractions of carbonate and organic carbon buried in sediments and changes in carbon sinks and sources may be reflected in marine carbon-isotope records (Kump and Arthur, 1999). Since carbonate is mostly produced in surface waters (Broecker and Woodruff, 1992; Kump, 1991), we use a compilation by Katz et al. (2005) of bulk sediment carbonate carbon isotopes, which mainly reflect calcareous plankton. A comparison between this bulk sediment $\delta^{13}C_{carb}$ record and the benthic foraminifera $\delta^{13}C_{BF}$ record compiled by Cramer et al. (2009) provides some insight into the evolving role of the biological pump, which describes the transfer of carbon from the shallow to deep water reservoirs. The compiled bulk sediment and benthic records are both reasonable continuous from ~ 77 Ma to Present and are plotted in Fig. 7.

The organic fraction (f_{org}) of the total carbon burial flux at steady state can be estimated using the relationship (Eq. 4 in Kump and Arthur, 1999):

$$f_{org} = (\delta'_w - \delta_{carb})/\Delta_B$$

where δ'_w is the average carbon isotopic composition of the volcanic and riverine flux (assumed to be −5‰), δ_{carb} is the isotopic composition of carbonate sediments that reflect the oceanic carbon reservoir, and Δ_B represents the isotopic difference between the organic matter and carbonate deposited from the ocean. If Δ_B is assumed to be constant (say −29‰) from 77 Ma to 15 Ma, when the rise of C_4 photosynthetic pathways may have influenced the organic carbon isotopic composition, a mean δ_{carb} of 2.3‰ would imply a mean organic burial fraction (f_{org}) of 0.25 over this time interval. Accounting for a photosynthetic isotope effect related to atmospheric pCO_2 (expressed as a dependence of Δ_B on ambient pCO_2; Kump and Arthur, 1999) would tend to slightly increase the average organic burial fraction with declining atmospheric pCO_2 levels since 35 Ma, for example, f_{org} would be 0.27 for pCO_2 of ∼ 350 ppm.

Two prominent features in the bulk sediment carbon isotope record deserve discussion. One is a huge fluctuation with a 1.5‰ increase starting at around 62.5 Ma that peaks at 57 Ma and plummeting by 2‰ to a prominent trough at 52 Ma (Fig. 7b). The run-up to the carbon isotope peak at 57 Ma implies an increasing fraction of organic carbon sequestration (f_{org} up to 0.3). This may be related to burial of organic-rich sediments deposited on the passive margin of Greater India encountering the equatorial high productivity belt during final stages of transit toward the Tethyan subduction zone (Fig. 3b); the subsequent decrease in carbonate carbon isotope values (implying that f_{org} decreased to more typical values of ∼ 0.22) starting at around 57 Ma may mark the exhumation and oxidation of these and other organic carbon-rich Tethyan marine sediments during the early stages of the India-Asia collision, as suggested by Beck et al. (1995). The climatic effect of this large perturbation is not entirely clear: Beck et al. (1995) suggested that exhumation of organic carbon from the Tethyan colliding margins may have increased atmospheric greenhouse gases sufficiently to have driven

global warming in the early Cenozoic even though the EECO seems to peak a few million years after the signature decrease in carbonate carbon isotope ratios (Fig. 7a).

The second notable perturbation is the large (up to ∼ 2.5‰) decrease in both the bulk sediment and benthic records from 15 Ma to present (Fig. 7b, c). This marked downward trend was originally interpreted by Shackleton (1987) as due to a decreasing fraction of organic carbon burial (ostensibly from 0.3 to 0.2) but even with validating data (Shackleton and Hall, 1995), its origin was considered rather enigmatic (Broecker and Woodruff, 1992). Katz et al. (2005) suggested that about 1.1‰ of the decrease in the bulk sediment carbon isotope record could be accounted for by the rise of C_4 photosynthetic pathways over the past 15 Myr with the remaining ∼ 1.4‰ decrease due to weathering of organic-rich shales. In any case, there is no evidence for increasing organic carbon burial over the past 15 Myr even though climate deteriorated from the Middle Miocene climate optimum (Flower and Kennett, 1994; Miller et al., 1987; Wright et al., 1992; You et al., 2009).

In a comparison between the bulk sediment and benthic carbonate $\delta^{13}C$ records (Fig. 7B, C), the average value for benthic data between 77 Ma and 65 Ma, just before the Cretaceous–Paleogene boundary perturbation (D'Hondt et al., 1998), is 1.14‰, which is 1.13‰ lighter than the bulk sediment $\delta^{13}C$ mean of 2.27‰ over the same interval. From 50 Ma, just after the Paleocene–Eocene boundary perturbation (Hilting et al., 2008), to 35 Ma, just before Oi-1 at around the Eocene–Oligocene boundary, the benthic mean is 0.70‰, which is now 1.56‰ lighter than the corresponding bulk sediment mean of 2.26‰. From 33 Ma, just after Oi-1, to 18 Ma, just before the Middle Miocene Climate Optimum, the benthic mean is 0.73‰ and again about 1.56‰ lighter than the corresponding bulk sediment mean of 2.29‰. It would thus appear that the biological pump spun-up soon after EECO (∼ 50 Ma), which is well before the strengthening of ocean circulation and the inception of large Antarctic ice sheets at Oi-1 at around 34 Ma (e.g., Cramer et al., 2009; Kennett, 1977). In fact, the deep water to surface water $\delta^{13}C$ gradient (a measure of biopump activity) was hardly different from 35–50 Ma to 18–33 Ma according to these data, indicating that there had to be

other processes besides the redistribution of nutrients by ocean circulation to account for the carbon isotope profiles. We suggest that higher biological productivity was plausibly spurred by influx of new nutrients, notably phosphate (Schrag et al., 2002), from enhanced weathering of continental silicates starting at EECO, which coincided with widespread deposition of chert in the world ocean (Muttoni and Kent, 2007).

We conclude that over the past 100 Myr (Late Cretaceous and Cenozoic), high organic carbon burial, such as major oil formation in the Cretaceous (Irving et al., 1974), seemed to be more in response to higher productivity associated with elevated atmospheric pCO_2 concentrations and resulting greater nutrient supply from continental silicate weathering but did not seem to play a very prominent role in modulating atmospheric pCO_2 over this time scale.

7 Uplift-erosion hypothesis

According to the uplift-erosion hypothesis (Raymo and Ruddiman, 1992), uplift of the Himalayas and Tibetan Plateau as a consequence of the India-Asia collision enhanced silicate weathering rates and the associated consumption of atmospheric pCO_2, causing Earth's climate to descend into glacial mode with the initiation of continental-scale ice sheets at $\sim$ 34 Ma. This was largely based on the supposition that the progressive increase in $^{87}Sr/^{86}Sr$ values of marine carbonates since $\sim$ 40 Ma (Richter et al., 1992) was due to enhanced delivery of radiogenic Sr due to increased global chemical weathering rates from mountain building, especially the uplift of the Himalayas (Raymo et al., 1988). Others have argued rather persuasively, however, that most of the overall increase in $^{87}Sr/^{86}Sr$ resulted from the unroofing and weathering erosion of particularly radiogenic Himalayan rocks, such as leucogranites (Edmond, 1992) and metasediments (Harris, 1995) including metamorphosed limestones (Quade et al., 1997), in which case the $^{87}Sr/^{86}Sr$ seawater curve may not serve as a simple proxy for global weathering rates of continental silicates. The Himalayas and Tibetan Plateau formed in the boreal arid belt (Fig. 3d), which along with adiabatically cooler temperatures due to

high elevations during uplift would not make them prime candidates for strong chemical weathering and high CO_2 consumption. Vigorous (weathering-limited) mechanical erosion occurred in elevated regions with high relief but silicate weathering intensity is generally low, even in the sediment basins like the Ganges system at lower elevations (France-Lanord and Derry, 1997).

We had previously suggested (Kent and Muttoni, 2008) that weathering of exhumed Himalayan silicates may have taken over as an important CO_2 sink as the Deccan Traps began to drift out of the equatorial humid belt, in basic agreement with the uplift-erosion hypothesis. However, while we firmly acknowledge the importance of relief in maintaining weatherable surfaces, we suggest that it is the potency of a warm and humid setting that is of greater importance in the overall consumption of CO_2. We would thus now argue that enhanced continental silicate weathering stemming from the emplacement of the Ethiopian Traps and especially the arrival and continued residence of SE Asia in the equatorial humid belt provides a better explanation for the subsequent drawing down of atmospheric pCO_2.

8 Implications for calcite and aragonite seas

Carbonate mineralogy has oscillated through the Phanerozic between low-Mg calcite and high-Mg conditions favoring aragonite deposition, with calcite seas usually associated with greenhouse climates (most recently from the Jurassic to Eocene) and aragonite seas with icehouse climates (most recently from Oligocene to Present) (Sandberg, 1983) (Fig. 7). The broad secular shifts in carbonate mineralogies coincide with oscillations in potash evaporite composition (Hardie, 1996) and are generally attributed to changes in Mg/Ca ratios of ancient seawater, which can be reconstructed from fluid inclusions (Lowenstein et al., 2001), fossil echinoderms (Dickson, 2002) and carbonate veins formed in oceanic crust (Coggon et al., 2010): all show a parallel albeit poorly dated rise in Mg/Ca ratios starting sometime in the mid-Cenozoic. Long-term oscillations in Mg/Ca ratios of seawater are typically modeled as being controlled primarily

by varying hydrothermal activity (a major Mg sink) driven by presumed changes in the rate of ocean crust production (Demicco et al., 2005; Farkas et al., 2007; Hardie, 1996; Stanley and Hardie, 1998). However, if rates of ocean crust production (and hydrothermal activity) were actually steady (Rowley, 2002), and barring major changes in other potential Mg-sinks like dolomitization, changes in sources of Mg and Ca may have played a significant role in influencing the major cation chemistry of sea water. In particular, the mid-Cenozoic increase in Mg/Ca ratios may be due to intense weathering of continental mafic rocks starting with the entry of the Deccan Traps into the equatorial humid belt at 50 Ma and continuing with that of the Ethiopian Traps and up to the present with the SE Asia arc terrane, essentially part of the same process that we believe caused the drawdown in atmospheric pCO_2. The Deccan's initial volume of $\sim 4\,\mathrm{Mkm}^3$ (Courtillot and Renne, 2003) means it alone contained roughly 360 Tton of Mg (nominal concentration of 3 wt %). Compared to (modern) riverine Mg flux equivalent to $\sim 140\,\mathrm{Mton\,yr}^{-1}$ (Holland, 1984), this suggests that erosion of the Deccan could have contributed important extra Mg for the calcite-aragonite sea transition as well as extra Ca that sensibly deepened the carbonate compensation depth over the later part of the Cenozoic (Lyle et al., 2008).

9 Transport-limited negative feedback

The relatively small surficial carbon reservoir compared to the large carbon fluxes implies that there is close parity on million year time scales between inputs (volcanic outgasssing and metamorphism) and outputs (silicate weathering followed by deposition of carbonate minerals and burial of organic carbon) to maintain a stable level of CO_2 in the atmosphere (Berner and Caldeira, 1997). This fine balance requires a negative feedback that depends strongly on the level of atmospheric CO_2. A powerful concept for policing the CO_2 content of the atmosphere is the CO_2-silicate weathering feedback mechanism of Walker et al. (1981) that underlies the BLAG model (Berner et al., 1983) and the GEOCARB lineage of supply-side carbon cycling models (Berner,

2004): increases or decreases in CO_2 outgassing induce an opposing response from higher or lower chemical weathering rates via associated greenhouse effects. A stabilizing negative feedback is more difficult to identify in a sink-side model, for example, an uplift-weathering mechanism (i.e., model of Raymo and Ruddiman, 1992) left uncoupled to the CO_2 content of the atmosphere would eventually produce a crash in atmospheric pCO_2. After evaluating alternative mechanisms, such as a possible albeit tenuous link between erosion and organic carbon burial (Raymo, 1994), Broecker and Sanyal (1998) concluded that the pCO_2 level of the atmosphere almost certainly has to act as the controller of a silicate weathering feedback.

So what is to keep atmospheric pCO_2 from plunging or wildly oscillating in our dynamic geography, sink-side model? We suggest that as a continental silicate province drifts into the equatorial humid belt and is subject to relatively intense chemical weathering, there may eventually be a transition from weathering-limited to transport-limited regimes with thickening of cation-deficient soils that will tend to retard further chemical weathering of the bedrock; this is likely to characterize cratonic areas with low relief (Kump et al., 2000; West et al., 2005). In the case of continental basaltic provinces entering the equatorial humid belt, they are provided with initial relief from plume head uplift and the stacking of lava flows that would prolong the weathering-limited phase; nevertheless, they may eventually be either consumed by intense weathering or drift out of the intense weathering regime, resulting in a reduction to their contribution to CO_2 drawdown. The Deccan and Ethiopian Traps soon enough drifted out of the equatorial humid belt and escaped this fate of complete consumption by weathering and erosion whereas most of the once widespread CAMP lavas were evidently largely consumed probably not long after their emplacement at around 201 Ma (Schaller et al., 2012), leaving only a few remnants amongst the now-dispersed Atlantic-bordering continents.

An interesting exception is SE Asia, a major CO_2 sink (Dessert et al., 2003) that has been straddling the equatorial humid belt since at least 25 Ma and which, as a set of island arc terranes, has been continuously rejuvenated by uplift and magmatism

and therefore subjected to persistent intense weathering. There would be hardly any negative feedback in this case, making SE Asia a prime candidate responsible for the unregulated consumption of enough CO_2 to plunge Earth's climate system into a glacial mode and keep it there in the later part of the Cenozoic. Higher east-west sea-surface temperature gradients and more vigorous Walker circulation in the equatorial Pacific, much like normal conditions today, resulted from the end of continual El Nino due to global shoaling of the oceanic thermocline at around 3 Ma (Fedorov et al., 2006; Ravelo, 2006); we are tempted to speculate that increased rainfall over the SE Asia equatorial archipelago may have caused sufficiently higher CO_2 consumption from runoff-enhanced silicate weathering to trigger Northern Hemisphere glaciations.

10 Concluding remarks

We conclude that while significant variations in potential sources of CO_2 such as oceanic crust production rates and hydrothermal activity cannot be precluded even though they are notoriously difficult to calibrate, a dynamic paleogeographic model of variable CO_2 sinks arising from the changing latitudinal distribution of land masses, and especially basaltic provinces and island arc terranes, provides a measurable and hence testable mechanism to account for long-term variations in atmospheric pCO_2 levels over the Late Cretaceous and Cenozoic, and potentially further back in Earth history.

Key is the sporadic presence of highly weatherable continental basalt provinces in the equatorial humid belt, the engine of Earth's climate system that is characterized by warm temperatures and high rainfall at widely varying atmospheric pCO_2 levels. With no highly weatherable basaltic provinces in the equatorial humid belt from at least 120 Ma to 50 Ma, atmospheric pCO_2 levels tended to be elevated giving rise to warm climates such as the intervals centered on the CTM and the EECO. These super-greenhouse conditions would have activated enhanced weathering of continents and especially basaltic provinces in a warmer and wetter temperate humid belt. For

example, many of the lavas of the British Tertiary igneous province, a subprovince of the North Atlantic igneous province LIP of Late Paleocene to Early Eocene age that was emplaced and remained at mid-paleolatitudes of $\sim 45^{\circ}$ N (Ganerød et al., 2010), were erupted subaerially (Saunders et al., 1997) and are often closely associated with well-developed laterites, such as the 30 m-thick unit belonging to the Interbasaltic Formation in Antrim, Northern Ireland (Hill et al., 2000) and the red boles on the Isles of Mull and Skye in Scotland (Emeleus et al., 1996). Elsewhere in ostensibly temperate Europe, bauxite was named from Les Baux-de-Provence in France ($\sim 44^{\circ}$ N) for a lateritic aluminum ore that mainly formed on carbonate rocks of Jurassic and Cretaceous age (Retallack, 2010). In western North America, some of the highest calculated denudation rates for crystalline bedrock for non-glacial times were documented in the Green River Basin (42° N) and ascribed to enhanced silicate dissolution rates associated with elevated atmospheric pCO_2 levels that occurred during the EECO (Smith et al., 2008).

These and other examples support the concept that basaltic provinces outside the equatorial humid belt effectively act as safety valves that limit extreme accumulations of CO_2 in the atmosphere. Nonetheless, a dynamic CO_2-sink model implies that equable climates are the norm or default mode. Ice ages are the exception, due to fortuitous latitudinal distributions of potent silicate weathering sinks of CO_2 with only weak negative feedback. In other words, the silicate-weathering thermostat, so effective at the high temperature end, sometimes cannot sufficiently decrease weathering rates of highly weatherable (i.e., basaltic) continental provinces in the equatorial humid belt that is not well coupled to atmospheric pCO_2 levels, thus paving the way to an ice age (or at the extreme, a Snowball Earth: Hoffman and Schrag, 2002; Godderis et al., 2003).

Acknowledgements. We thank our respective institutions for their support that allowed us to accomplish this bootlegged research. We especially acknowledge constructive comments and informative discussions after presentations of evolving versions of this work that challenged us to look deeper and more broadly at the problem. In particular, we are grateful to Ben Cramer, Bob Kopp, Peter Molnar and Morgan Schaller for detailed written comments, and Wally Broecker, Mimi Katz and Ken Miller for valuable critical exchanges on earlier versions of the manuscript. Ben Cramer and Mimi Katz generously provided digital files of compiled carbon isotope data. Lamont-Doherty Earth Observatory contribution #0000.

References

Achache, J., Courtillot, V., and Zhou, Y. X.: Paleogeographic and tectonic evolution of Southern Tibet since middle Cretaceous time: new paleomagnetic data and synthesis, J. Geophys. Res., 89, 10311–10339, 1984.

Agard, P., Omrani, J., Jolivet, L., and Mouthereau, G.: Convergence history across Zagros (Iran): constraints from collisional and earlier deformation, Int. J. Earth Sci., 94, 401– 419, 2005.

Aitchison, J. C., Ali, J. R., and Davis, A. M.: When and where did India and Asia collide?, J. Geophys. Res., 112, B05423, doi:10.1029/2006JB004706, 2007.

Aitchison, J. C., Ali, J. R., and Davis, A. M.: Reply to comment by Eduardo Garzanti on "When and where did India and Asia collide?", J. Geophys. Res., 113, B04412, doi:10.1029/2007JB005431, 2008.

Ali, J. R. and Aitchison, J. C.: Gondwana to Asia: plate tectonics, paleogeography and the biological connectivity of the Indian sub-continent from the Middle Jurassic through latest Eocene (166–35 Ma), Earth-Sci. Rev., 88, 145–166, 2008.

Allègre, C. J., Courtillot, V., Tapponnier, P., Hirn, A., Mattauer, M., Coulon, C., Jaeger, J. J., Achache, J., Scharer, U., Marcoux, J., Burg, J. P., Girardeau, J., Armijo, R., Gariepy, C., Gopel, C., Tindong, L., Xuchang, X., Chenfa, C., Guangqin, L., Baoyu, L., Jiwen, T., Naiwen, W., Guoming, C., Tonglin, H., Xibin, W., Wanming, D., Huaibin, S., Yougong, C., Ji, Z., Hongrong, Q., Peisheng, B., Songchan, W., Bixiang, W., Yaoxiu, Z., and Xu, R.: Structure and evolution of the Himalaya-Tibet orogenic belt, Nature, 307, 17–22, 1984.

Allen, M. B. and Armstrong, H. A.: Arabia-Eurasia collision and the forcing of mid-Cenozoic global cooling, Palaeogeogr. Palaeocl., 265, 52–58, 2008.

Beck, R. A., Burbank, D. W., Sercombe, W. J., Olson, T. L., and Khan, A. M.: Organic carbon exhumation and global warming during the early Himalayan collision, Geology, 23, 387–390, 1995.

Beerling, D. J. and Royer, D. L.: Convergent Cenozoic CO_2 history, Nat. Geosci., 4, 418–420, 2011.

Berger, W. H. and Winterer, E. L.: Plate stratigraphy and the fluctuating carbonate line, in: Pelagic Sediments: On Land and Under the Sea, edited by: Hsu, K. J. and Jenkins, H. C., Special Publications of the International Association of Sedimentologists, No. 1, Blackwell Scientific Publications, Oxford, 11–48, 1974.

Berner, R. A.: Global CO_2 degassing and the carbon cycle: comment on "Cretaceous ocean crust at DSDP sites 417 and 418: carbon uptake from weathering vs. loss by magmatic outgassing", Geochim. Cosmochim. Acta, 54, 2889–2890, 1990a.

Berner, R. A.: Response to criticism of the BLAG model, Geochim. Cosmochim. Acta, 54, 2893, 1990b.

Berner, R. A.: A model for atmospheric CO_2 over Phanerozoic time, Am. J. Sci., 291, 339–376, 1991.

Berner, R. A.: GEOCARB II: a revised model of atmospheric CO_2 over Phanerozoic time, Am. J. Sci., 294, 56–91, 1994.

Berner, R. A.: The Phanerozoic Carbon Cycle, Oxford University Press, Oxford, 150 pp., 2004.

Berner, R. A.: GEOCARBSULF: a combined model for Phanerozoic atmospheric O_2 and CO_2, Geochim. Cosmochim. Acta, 70, 5653–5664, 2006.

Berner, R. A. and Caldeira, K.: The need for mass balance and feedback in the geochemical carbon cycle, Geology, 25, 955–956, 1997.

Berner, R. A. and Kothalava, Z.: GEOCARB III: a revised model of atmospheric CO_2 over Phanerozoic time, Am. J. Sci., 301, 182–204, 2001.

Berner, R. A., Lasaga, A. C., and Garrels, R. M.: The carbonate-silicate geochemical cycle and its effect on atmospheric carbon dioxide over the past 100 million years, Am. J. Sci., 283, 641–683, 1983.

Besse, J. and Courtillot, V.: Apparent and true polar wander and the geometry of the geomagnetic field over the last 200 Myr, J. Geophys. Res., 107, 2300, doi:10.1029/2000JB000050, 2002.

Besse, J. and Courtillot, V.: Correction to "Apparent and true polar wander and the geometry of the geomagnetic field over the last 200 Myr", J. Geophys. Res., 108, 2469, doi:10.1029/2003JB002684, 2003.
Brady, P. V. and Gislason, S. R.: Seafloor weathering controls on atmospheric CO_2 and global climate, Geochim. Cosmochim. Acta, 61, 965–973, 1997.
Briais, A., Patriat, P., and Tapponnier, P.: Updated interpretation of magnetic anomalies and seafloor spreading stages in the South China Sea: implications for the Tertiary tectonics of Southeast Asia, J. Geophys. Res., 98, 6299–6328, 1993.
Broecker, W. S. and Sanyal, A.: Does atmospheric CO_2 police the rate of chemical weathering?, Global Biogeochem. Cy., 12, 403–408, 1998.
Broecker, W. S. and Woodruff, F.: Discrepancies in the oceanic carbon isotope record for the last fifteen million years?, Geochim. Cosmochim. Acta, 56, 3259–3264, 1992.
Caldeira, K.: Enhanced Cenozoic chemical weathering and the subduction of pelagic carbonate, Nature, 357, 578–581, 1992.
Caldeira, K. and Rampino, M. R.: Carbon dioxide emissions from Deccan volcanism and a K/T boundary greenhouse effect, Geophys. Res. Lett., 17, 1299–1302, 1990.
Cande, S. C. and Kent, D. V.: Revised calibration of the geomagnetic polarity time scale for the Late Cretaceous and Cenozoic, J. Geophys. Res., 100, 6093–6095, 1995.
Cande, S. C. and Stegman, D. R.: Indian and African plate motions driven by the push force of the Reunion plume head, Nature, 475, 47–52, 2011.
Chang, C.-F. and Cheng, H.-L.: Some tectonic features of the Mt. Jolmo Lungma area, Southern Tibet, China, Sci. Sin., 16, 257–265, 1973.
Chen, W., Yang, T., Zhang, S., Yang, Z., Li, H., Wu, H., Zhang, J., Ma, Y., and Cai, F.: Paleomagnetic results from the Early Cretaceous Zenong Group volcanic rocks, Cuoqin, Tibet, and their paleogeographic implications, Gondwana Res., 22, 461–469, 2012.
Chen, Y., Courtillot, V., Cogne, J.-P., Besse, J., Yang, Z., and Enkin, R. J.: The configuration of Asia prior to the collision of India: Cretaceous paleomagnetic constraints, J. Geophys. Res., 98, 21927–21941, 1993.
Coggon, R. M., Teagle, D. A. H., Smith-Duque, C. E., Alt, J. C., and Cooper, M. J.: Reconstructing past seawater Mg/Ca and Sr/Ca from mid-ocean ridge flank calcium carbonate veins, Science, 327, 1114–1117, 2010.

Cogné, J. P.: PaleoMac: A Macintosh™ application for treating paleomagnetic data and making plate reconstructions, Geochem. Geophy. Geosy., 4, 1007, doi:10.1029/2001GC000227, 2003.
Cogné, J.-P. and Humler, E.: Temporal variation of oceanic spreading and crustal production rates during the last 180 My, Earth Planet. Sc. Lett., 227, 427–439, 2004.
Cogné, J. P. and Humler, E.: Trends and rhythms in global seafloor generation rate, Geochem. Geophy. Geosy., 7, Q03011, doi:10.1029/2005GC001148, 2006.
Copley, A., Avouac, J.-P., and Royer, J.-Y.: India-Asia collision and the Cenozoic slowdown of the Indian plate: Implications for the forces driving plate motions, J. Geophys. Res., 115, B03410, doi:10.1029/2009JB006634, 2010.
Courtillot, V. E. and Renne, P. R.: On the ages of flood basalt events, C. R. Geosci., 335, 113–140, 2003.
Cramer, B. S., Toggweiler, J. R., Wright, J. D., Katz, M. E., and Miller, K. G.: Ocean overturning since the Late Cretaceous: Inferences from a new benthic foraminiferal isotope compilation, Paleoceanography, 24, PA4216, doi:10.1029/2008PA001683, 2009.
Cramer, B. S., Miller, K. G., Toggweiler, J. R., Barrett, P. J., and Wright, J. D.: Late Cretaceous-Neogene trends in deep ocean temperature and continental ice volume: reconciling records of benthic foraminiferal geochemistry ($\delta^{18}O$ and Mg/Ca) with sea level history, J. Geophys. Res.-Oceans, 116, C12023, doi:10.1029/2011JC007255, 2011.
DeConto, R. M. and Pollard, D.: Rapid Cenozoic glaciation of Antarctica induced by declining atmospheric CO_2, Nature, 421, 245–249, 2003.
DeConto, R. M., Pollard, D., Wilson, P. A., Palike, H., Lear, C. H., and Pagani, M.: Thresholds for Cenozoic bipolar glaciation, Nature, 455, 652–656, 2008.
Demicco, R. V., Lowenstein, T. K., Hardie, L. A., and Spencer, R. J.: Model of seawater composition for the Phanerozoic, Geology, 33, 877–880, 2005.
Dessert, C., Dupré, B., Francois, L. M., Schott, J. J., Gaillardet, J., Chakrapani, G., and Bajpai, S.: Erosion of Deccan Traps determined by river geochemistry: impact on the global climate and the 87Sr/86Sr ratio of seawater, Earth Planet. Sc. Lett., 188, 459–474, 2001.
Dessert, C., Dupré, B., Gaillardet, J., Francois, L., and Allègre, C.: Basalt weathering laws and the impact of basalt weathering on the global carbon cycle, Chem. Geol., 202, 257–273, 2003.

D'Hondt, S., Donaghay, P., Zachos, J. C., Luttenberg, D., and Lindinger, M.: Organic carbon fluxes and ecological recovery from the Cretaceous–Tertiary mass extinction, Science, 282, 276–279, 1998.
Dickson, J. A. D.: Fossil echinoderms as monitor of the Mg/Ca ratio of Phanerozoic oceans, Science, 298, 1222–1224, 2002.
Donnadieu, Y., Goddéris, Y., Pierrehumbert, R., Dromart, G., Fluteau, F., and Jacob, R.: A GEOCLIM simulation of climatic and biogeochemical consequences of Pangea breakup, Geochem. Geophy. Geosy., 7, Q11019, doi:10.1029/2006GC001278, 2006.
Dupont-Nivet, G., Lippert, P. C., Van Hinsbergen, D. J. J., Meijers, M. J. M., and Kapp, P.: Palaeolatitude and age of the Indo–Asia collision: palaeomagnetic constraints, Geophys. J. Int., 182, 1189–1198, 2010.
Dupré, B., Dessert, C., Oliva, P., Goddéris, Y., Viers, J., François, L., Millot, R., and Gaillardet, J.: Rivers, chemical weathering and Earth's climate, C. R. Geosci., 335, 1141–1160, 2003.
Edmond, J. M.: Himalayan tectonics, weathering processes, and the strontium isotope record in marine limestones, Science, 258, 1594–1597, 1992.
Edmond, J. M. and Huh, Y.: Non-steady state carbonate recycling and implications for the evolution of atmospheric pCO_2, Earth Planet. Sc. Lett., 216, 125–139, 2003.
Emeleus, C. H., Allwright, E. A., Kerr, A. C., and Williamson, I. T.: Red tuffs in the Palaeocene lava successions of the Inner Hebrides, Scott. J. Geol., 32, 83–89, 1996.
Engebretson, D. C., Kelley, K. P., Cashman, H. J., and Richards, M. A.: 180 million years of subduction, GSA Today, 2, 93–95, 1992.
Erba, E.: Calcareous nannofossils and Mesozoic oceanic anoxic events, Mar. Micropaleontol., 52, 85–106, 2004.
Farkas, J., Bohm, F., Wallmann, K., Blenkinsop, J., Eisenhauer, A., van Geldern, R., Munnecke, A., Voigt, S., and Veizer, J.: Calcium isotope record of Phanerozoic oceans: implications for chemical evolution of seawater and its causative mechanisms, Geochim. Cosmochim. Acta, 71, 5117–5134, 2007.
Fedorov, A. V., Dekens, P. S., McCarthy, M., Ravelo, A. C., deMenocal, P. B., Barreiro, M., Pacanowski, R. C., and Philander, S. G.: The Pliocene paradox (mechanisms for a permanent El Nino), Science, 312, 1485–1499, 2006.
Flower, B. P. and Kennett, J. P.: The middle Miocene climatic transition: East Antarctic ice sheet development, deep ocean circulation and global carbon cycling, Palaeogeogr. Palaeocl., 108, 537–555, 1994.

France-Lanord, C. and Derry, L. A.: Organic carbon burial forcing of the carbon cycle from Himalayan erosion, Nature, 390, 65–67, 1997.
Fuller, M., Ali, J. R., Moss, S. J., Frost, G. M., Richter, B., and Mahfi, A.: Paleomagnetism of Borneo, J. Asian Earth Sci., 17, 3–24, 1999.
Gaillardet, J., Dupré, B., Louvat, P., and Allègre, C. J.: Global silicate weathering and CO_2 consumption rates deduced from the chemistry of large rivers, Chem. Geol., 159, 3–30, 1999.
Ganerød, M., Smethurst, M. A., Torsvik, T. H., Prestvik, T., Rousse, S., McKenna, C., Hinsbergen, J. J., and Hendriks, B. W. H.: The North Atlantic Igneous Province reconstructed and its relation to the Plume Generation Zone: the Antrim Lava Group revisited, Geophys. J. Int., 182, 183–202, 2010.
Garzanti, E.: Comment on "When and where did India and Asia collide?" by Jonathan C. Aitchison, Jason R. Ali, and Aileen M. Davis, J. Geophys. Res., 113, B004411, doi:10.1029/2007JB005276, 2008.
Garzanti, E., Baud, A., and Mascle, G.: Sedimentary record of the northward flight of India and its collision with Eurasia (Ladakh Himalaya, India), Geodinamica Acta (Paris), 1, 297–312, 1987.
Gerlach, T.: Volcanic versus anthropogenic carbon dioxide, EOS, Transactions, American Geophysical Union, 92, 201–202, 2011.
Godderis, Y., Donnadieu, Y., Nedelec, A., Dupre, B., Dessert, C., Grard, A., Ramstein, G., and Francois, L. M.: The Sturtian "snowball" glaciation: fire and ice, Earth Planet. Sc. Lett., 211, 1–12, 2003.
Godderis, Y., Donnadieu, Y., de Vargas, C., Pierrehumbert, R. T., Dromart, G., and van de Schootbrugge, B.: Causal or casual link between the rise of nannoplankton calcification and a tectonically-driven massive decrease in Late Triassic atmospheric CO_2?, Earth Planet. Sc. Lett., 267, 247–255, 2008.
Hall, R., vanHattum, M. W. A., and Spakman, W.: Impact of India–Asia collision on SE Asia: the record in Borneo, Tectonophysics, 451, 366–389, 2008.
Hansen, J., Sato, M., Kharecha, P., Beerling, D., Berner, R., Masson-Delmotte, V., Pagani, M., Raymo, M., Royer, D. L., and Zachos, J. C.: Target atmospheric CO_2: where should humanity aim?, Open Atmos. Sci. J., 2, 217–231, 2008.

Hardie, L. A.: Secular variation in seawater chemistry: an explanation for the coupled secular variation in the mineralogies of marine limestones and potash evaporites over the past 600 m.y, Geology, 24, 279–283, 1996.
Harris, N.: Significance of weathering Himalayan metasedimentary rocks and leucogranites for the Sr isotope evolution of seawater during the early Miocene, Geology, 23, 795–798, 1995.
Hatzfeld, D. and Molnar, P.: Comparisons of the kinematics and deep structures of the Zagros and Himalaya and of the Iranian and Tibetan plateaus and geodynamic implications, Rev. Geophys., 48, RG2005, doi:10.1029/2009RG000304, 2010.
Hill, I. G., Worden, R. H., and Meighan, I. G.: Geochemical evolution of a palaeolaterite: the Interbasaltic Formation, Northern Ireland, Chem. Geol., 166, 65–84, 2000.
Hilting, A. K., Kump, L. R., and Bralower, T. J.: Variations in the oceanic vertical carbon isotope gradient and their implications for the Paleocene-Eocene biological pump, Paleoceaeanography, 23, PA3222, doi:10.1029/2007PA001458, 2008.
Hoffman, P. F. and Schrag, D. P.: The snowball Earth hypothesis: testing the limits of global change, Terra Nova, 14, 129–155, 2002.
Holland, H. D.: The Chemical Evolution of the Atmosphere and Oceans, Princeton University Press, Princeton, p. 582, 1984.
Irving, E., North, F. K., and Couillard, R.: Oil, climate and tectonics, Can. J. Earth Sci., 11, 1–17, 1974.
Johnston, F. K. B., Turchyn, A. V., and Edmonds, M.: Decarbonation efficiency in subduction zones: implications for warm Cretaceous climates, Earth Planet. Sc. Lett., 303, 143–152, 2011.
Katz, M. E., Wright, J. D., Miller, K. G., Cramer, B. S., Fennel, K., and Falkowski, P. G.: Biological overprint of the geological carbon cycle, Mar. Geol., 217, 323–338, 2005.
Kennett, J. P.: Cenozoic evolution of Antarctic glaciation, the circum-antarctic ocean and their impact on global paleoceanography, J. Geophys. Res., 82, 3843–3860, 1977.
Kent, D. V. and Irving, E.: Influence of inclination error in sedimentary rocks on the Triassic and Jurassic apparent polar wander path for North America and implications for Cordilleran tectonics, J. Geophys. Res., 115, B10103, doi:10.1029/2009JB007205, 2010.
Kent, D. V. and Muttoni, G.: Equatorial convergence of India and early Cenozoic climate trends, Proc. Natl. Acad. Sci. USA, 105, 16065–16070, 2008.
Kump, L. R.: Interpreting carbon-isotope excursions: Strangelove oceans, Geology, 19, 299–302, 1991.

Kump, L. R. and Arthur, M. A.: Interpreting carbon-isotope excursions: carbonates and organic matter, Chem. Geol., 161, 181–198, 1999.
Kump, L. R., Brantley, S. L., and Arthur, M. A.: Chemical weathering, atmospheric CO_2, and climate, Ann. Rev. Earth Planet. Sci., 28, 611–667, 2000.
Lippert, P. C., Zhao, X., Coe, R. S., and Lo, C.-H.: Palaeomagnetism and 40Ar/39Ar geochronology of upper Palaeogene volcanic rocks from Central Tibet: implications for the Central Asia inclination anomaly, the palaeolatitude of Tibet and post-50 Ma shortening within Asia, Geophys. J. Int., 184, 131–161, 2011.
Livermore, R., Hillenbrand, C. D., Meredith, M., and Eagles, G.: Drake Passage and Cenozoic climate: an open and shut case?, Geochem. Geophy. Geosy., 8, Q01005, doi:10.1029/2005GC001224, 2007.
Lowenstein, T. K., Timofeeff, M. N., Brennan, S. T., Hardie, L. A., and Demicco, R. V.: Oscillations in Phanerozoic seawater chemistry: evidence from fluid inclusions, Science, 294, 1086–1088, 2001.
Lunt, D. J., Foster, G. L., Haywood, A. M., and Stone, E. J.: Late Pliocene Greenland glaciation controlled by a decline in atmospheric CO_2 levels, Nature, 454, 1102–1105, 2008.
Lyle, M., Barron, J., Bralower, T. J., Huber, M., Olivarez Lyle, A., Ravelo, A. C., Rea, D. K., and Wilson, P. A.: Pacific Ocean and Cenozoic evolution of climate, Rev. Geophys., 46, RG2002, doi:10.1029/2005RG000190, 2008.
Manabe, S. and Bryan, K.: CO_2-induced change in a coupled ocean-atmosphere model and its paleoclimatic implications, J. Geophys. Res., 90, 11689–11707, 1985.
Marty, B. and Tolstikhin, I. N.: CO_2 fluxes from mid-ocean ridges, arcs and plumes, Chem. Geol., 145, 233–248, 1998.
Marzoli, A., Renne, P. R., Piccirillo, E. M., Ernesto, M., Gellieni, G., and De Min, A.: Extensive 200-million-year-old continental flood basalts of the Central Atlantic Magmatic Province, Science, 284, 616–618, 1999.
McHone, J. G.: Volatile emissions from Central Atlantic Magmatic Province basalts: mass assumptions and environmental consequences, in: The Central Atlantic Magnatic Province: Insights from Fragments of Pangea, edited by: Hames, W. E., McHone, J. G., Renne, P. R., and Ruppel, C., Geophysical Monograph 136, American Geophysical Union, Washington, D.C., 241–254, 2003.
Miller, K. G., Fairbanks, R. G., and Mountain, G. S.: Tertiary oxygen isotope synthesis, sea level history, and continental margin erosion, Paleoceanography, 2, 1–19, 1987.

Miller, K. G., Kominz, M. A., Browning, J. V., Wright, J. D., Mountain, G. S., Katz, M. E., Sugarman, P. J., Cramer, B. S., Christie-Blick, N., and Pekar, S. F.: The Phanerozoic record of global sea-level change, Science, 310, 1293–1298, 2005a.

Miller, K. G., Wright, J. D., and Browning, J. V.: Visions of ice sheets in a greenhouse world, Mar. Geol., 217, 215–231, 2005b.

Misumi, K., Yamanaka, Y., and Tajika, E.: Numerical simulation of atmospheric and oceanic biogeochemical cycles to an episodic CO_2 release event: Implications for the cause of mid-Cretaceous Ocean Anoxic Event-1a, Earth Planet. Sc. Lett., 286, 316–323, 2009.

Mitchell, N. C. and Lyle, M. W.: Patchy deposits of Cenozoic pelagic sediments in the Central Pacific, Geology, 33, 49–52, 2005.

Mitchell, N. C., Lyle, M. W., Knappenberger, M. B., and Liberty, L. M.: Lower Miocene to Present stratigraphy of the equatorial Pacific sediment bulge and carbonate dissolution anomalies, Paleoceanography, 18, 1038, doi:10.1029/2002PA000828, 2003.

Moghadam, H. S., Whitechurch, H., Rahgoshay, M., and Monsef, I.: Significance of Nain-Baft ophiolitic belt (Iran): short-lived, transtensional Cretaceous back-arc oceanic basins over the Tethyan subduction zone, C. R. Geosci., 341, 1016–1028, 2009.

Molnar, P. and Stock, J. M.: Slowing of India's convergence with Eurasia since 20 Ma and its implications for Tibetan mantle dynamics, Tectonics, 28, TC3001, doi:10.1029/2008TC002271, 2009.

Molnar, P. and Tapponnier, P.: Cenozoic tectonics of Asia: effects of a continental collision, Science, 189, 419–426, 1975.

Muller, R. D. and Roest, W. R.: Fracture zones in the North Atlantic from combined Geosat and Seasat data, J. Geophys. Res., 97, 3337–3350, 1992.

Muller, R. D., Royer, J. Y., and Lawver, L. A.: Revised plate motions relative to the hotspots from combined Atlantic and Indian Ocean hotspot tracks, Geology, 21, 275–278, 1993.

Muller, R. D., Sdrolias, M., Gaina, C., Steinberger, B., and Heine, C.: Long-term sea-level fluctuations driven by ocean basin dynamics, Science, 319, 1357–1362, 2008.

Muttoni, G. and Kent, D. V.: Widespread formation of cherts during the early Eocene climate optimum, Palaeogeogr. Palaeocl., 253, 348–362, 2007.

Muttoni, G., Mattei, M., Balini, M., Zanchi, A., Gaetani, M., and Berra, F.: The drift history of Iran from the Ordovician to the Triassic, Geol. Soc. Spec. Publ., 312, 7–29, 2009.

Ogg, J. G., Karl, S. M., and Behl, R. J.: Jurassic through Early Cretaceous sedimentation history of the Central Equatorial Pacific and of Sites 800 and 801, Proceedings Ocean Drilling Program, Scientific Results, 129, 571–613, 1992.

Okay, A. I., Zattin, M., and Cavazza, W.: Apatite fission-track data for the Miocene Arabia-Eurasia collision, Geology, 38, 35–38, 2010.

Pagani, M., Zachos, J. C., Freeman, K. H., Tipple, B., and Bohaty, S.: Marked decline in atmospheric carbon dioxide concentrations during the Paleogene, Science, 309, 600–603, 2005.

Pagani, M., Huber, M., Liu, Z., Bohaty, S. M., Henderiks, J., Sijp, W., Krishnan, S., and DeConto, R. M.: The role of carbon dioxide during the onset of Antarctic glaciation, Science, 334, 1261–1264, 2011.

Patriat, P. and Achache, J.: India-Eurasia collision chronology has implications for crustal shortening and driving mechanism of plates, Nature, 311, 615–621, 1984.

Pearson, P. N., Ditchfield, P. W., Singano, J., Harcourt-Brown, K. G., Nicholas, C. J., Olsson, R. K., Shackleton, N. J., and Hall, M. A.: Warm tropical sea surface temperatures in the Late Cretaceous and Eocene epochs, Nature, 413, 481–488, 2001.

Pearson, P. N., vanDongen, B. E., Nicholas, C. J., Pancost, R. D., Schouten, S., Singano, J. M., and Wade, B. S.: Stable warm tropical climate through the Eocene Epoch, Geology, 35, 211–214, 2007.

Quade, J., Roe, L., DeCelles, P. G., and Ojha, T. P.: The Late Neogene 87Sr/86Sr record of lowland Himalayan rivers, Science, 276, 1828–1831, 1997.

Rabinowitz, P. D., Coffin, M. F., and Falvey, D.: The separation of Madagascar and Africa, Science, 220, 67–69, 1983.

Ravelo, A. C.: Walker circulation and global warming: lessons from the geologic past, Oceanography, 19, 114–122, 2006.

Raymo, M. E.: The Himalayas, organic carbon burial, and climate in the Miocene, Paleoceanography, 9, 399–404, 1994.

Raymo, M. E. and Ruddiman, W. F.: Tectonic forcing of late Cenozoic climate, Nature, 359, 117–122, 1992.

Raymo, M. E., Ruddiman, W. F., and Froelich, P. N.: Influence of late Cenozoic mountain building on ocean geochemical cycles, Geology, 16, 649–653, 1988.

Rea, D. K., Zachos, J. C., Owen, R. M., and Gingerich, P. D.: Global change at the Paleocene-Eocene boundary: climatic and evolutionary consequences of tectonic events, Palaeogeogr. Palaeocl., 79, 117–128, 1990.

Replumaz, A. and Tapponnier, P.: Reconstruction of the deformed collision zone between India and Asia by backward motion of lithospheric blocks, J. Geophys. Res., 108, 2285, doi:10.1029/2001JB000661, 2003.
Retallack, G. J.: Lateritization and bauxitization events, Econ. Geol., 105, 655–667, 2010.
Richter, B., Schmidtke, E., Fuller, M., Harbury, N., and Samsudin, A. R.: Paleomagnetism of Peninsular Malaysia, J. Asian Earth Sci., 17, 477–519, 1999.
Richter, F. M., Rowley, D. B., and DePaolo, D. J.: Sr isotope evolution of seawater: the role of tectonics, Earth Planet. Sc. Lett., 109, 11–23, 1992.
Rowley, D. B.: Rate of plate creation and destruction: 180 Ma to present, Geol. Soc. Am. Bull., 114, 927–933, 2002.
Rowley, D. B.: Extrapolating oceanic age distributions: lessons from the Pacific Region, J. Geol., 116, 587–598, 2008.
Royden, L. H., Burchfiel, B. C., and van der Hilst, R. D.: The geological evolution of the Tibetan Plateau, Science, 321, 1054–1058, 2008.
Royer, D. L.: Fossil soils constrain ancient climate sensitivity, P. Natl. Acad. Sci. USA, 107, 517–518, 2010.
Sandberg, P. A.: An oscillating trend in Phanerozoic non-skeletal carbonate mineralogy, Nature, 305, 19–22, 1983.
Saunders, A. D., Fitton, J. G., Kerr, A. C., Norry, M. J., and Kent, R. W.: The North Atlantic Igneous Province, in: Large Igneous Provinces: Continental, Oceanic, and Planetary Flood Volcanism, edited by: Mahoney, J. J. and Coffin, M. F., Geophysical Monograph 100, American Geophysical Union, Washington, D. C., 45–93, 1997.
Schaller, M. F., Wright, J. D., and Kent, D. V.: Atmospheric pCO_2 perturbations associated with the Central Atlantic Magmatic Province, Science, 331, 1404–1409, 2011.
Schaller, M. F., Wright, J. D., Kent, D. V., and Olsen, P. E.: Rapid emplacement of the Central Atlantic Magmatic Province as a net sink for CO_2, Earth Planet. Sc. Lett., 323–324, 27–39, 2012.
Schmidtke, E., Fuller, M., and Haston, R.: Paleomagnetic data from Sarawak, Malaysian Borneo and the Late Mesozoic and Cenozoic tectonics of Sundaland, Tectonics, 9, 123–140, 1990.
Schrag, D. P.: Control of atmospheric CO_2 and climate through Earth history, Geochim. Cosmochim. Acta, 66, A688, 2002.
Schrag, D. P., Berner, R. A., Hoffman, P. F., and Halverson, G. P.: On the initiation of a snowball Earth, Geochem. Geophy. Geosy., 3, 1036, doi:10.1029/2001GC000219, 2002.

Self, S., Thordarson, T., and Widdowson, M.: Gas fluxes from flood basalt eruptions, Elements, 1, 283–287, 2005.
Selverstone, J. and Gutzler, D. S.: Post-125 Ma carbon storage associated with continent-continent collision, Geology, 21, 885–888, 1993.
Seton, M., Gaina, C., Muller, R. D., and Heine, C.: Mid-Cretaceous seafloor spreading pulse: fact or fiction?, Geology, 37, 687–690, 2009.
Shackleton, N. J.: The carbon isotope record of the Cenozoic: history of organic carbon burial and of oxygen in the ocean and atmosphere, Geol. Soc. Spec. Publ., 26, 423–434, 1987.
Shackleton, N. J. and Hall, M. A.: Stable isotope records in bulk sediments (Leg 138), Proceedings Ocean Drilling Program, Sci. Res., 138, 797–805, 1995.
Smith, A. G. and Hallam, A.: The fit of the southern continents, Nature, 225, 139–144, 1970.
Smith, M. E., Carroll, A. R., and Mueller, E. R.: Elevated weathering rates in the Rocky Mountains during the Early Eocene Climatic Optimum, Nat. Geosci., 1, 370–374, 2008.
Srivastava, S. P. and Tapscott, C. R.: Plate kinematics of the North Atlantic, in: The Geology of North America, The Western North Atlantic Region, M, Geological Society of America, Boulder, 379–404, 1986.
Stanley, S. M. and Hardie, L. A.: Secular oscillations in the carbonate mineralogy of reef-building and sediment-producing organisms driven by tectonically forced shifts in seawater chemistry, Palaeogeogr. Palaeocl., 144, 3–19, 1998.
Staudigel, H., Hart, S. R., Schmincke, H.-U., and Smith, B. M.: Cretaceous ocean crust at DSDP Sites 417 and 418: carbon uptake from weathering versus loss by magmatic outgassing, Geochim. Cosmochim. Acta, 53, 3091–3094, 1989.
Staudigel, H., Hart, S. R., Schmincke, H.-U., and Smith, B. M.: Reply to "Global CO_2 degassing and the carbon cycle": a comment by Berner, R. A., Geochim. Cosmochim. Acta, 54, 2891, 1990a.
Staudigel, H., Hart, S. R., Schmincke, H.-U., and Smith, B. M.: Reply to R. A. Berner's response, Geochim. Cosmochim. Acta, 54, 2893, 1990b.
Stickley, C. E., Brinkhuis, H., Shellenberg, S. A., Sluijs, A., Rohl, U., Fuller, M., Grauert, M., Huber, M., Warnaar, J., and Williams, G. L.: Timing and nature of the deepening of the Tasmanian Gateway, Paleoceanography, 19, PA4027, doi:10.1029/2004PA001022, 2004.
Tejada, M. L. G., Suzuki, K., Kuroda, J., Coccioni, R., Mahoney, J. J., Ohkouchi, N., Sakamoto, T., and Tatsumi, Y.: Ontong Java Plateau eruption as a trigger for the early Aptian oceanic anoxic event, Geology, 37, 855–858, 2009.

Tera, F., Brown, L., Morris, J., Sacks, I. S., Klein, J., and Middleton, R.: Sediment incorporation in island-arc magmas: inferences from 10Be, Geochim. Cosmochim. Acta, 50, 535–550, 1986.

Thomas, D. J. and Bralower, T. J.: Sedimentary trace element constraints on the role of North Atlantic Igneous Province volcanism in late Paleocene-early Eocene environmental change, Mar. Geol., 217, 233–254, 2005.

Volk, T.: Sensitivity of climate and atmospheric CO_2 to deep-ocean and shallow-ocean carbonate burial, Nature, 337, 637–640, 1989.

Walker, J. C. G., Hays, P. B., and Kasting, J. F.: A negative feedback mechanism for the long-term stabilization of Earth's surface-temperature, J. Geophys. Res.-Atmos., 86, 9776–9782, 1981.

West, A. J., Galy, A., and Bickle, M.: Tectonic and climatic controls on silicate weathering, Earth Planet. Sc. Lett., 235, 211–228, 2005.

Wilkinson, B. H. and Walker, J. C. G.: Phanerozoic cycling of sedimentary carbonate, Am. J. Sci., 289, 525–548, 1989.

Wilson, P. A., Norris, R. D., and Cooper, M. J.: Testing the Cretaceous greenhouse hypothesis using glassy foraminiferal calcite from the core of the Turonian tropics on Demerara Rise, Geology, 30, 607–610, 2002.

Wright, J. D., Miller, K. G., and Fairbanks, R. G.: Early and Middle Miocene stable isotopes: implications for deepwater circulation and climate, Paleoceanography, 7, 357–389, 1992.

Yang, Z. and Besse, J.: Paleomagnetic study of Permian and Mesozoic sedimentary rocks from Northern Thailand supports the extrusion model for Indochina, Earth Planet. Sc. Lett., 117, 525–552, 1993.

Yang, Z., Yin, J., Sun, Z., Otofuji, Y.-I., and Sato, K.: Discrepant Cretaceous paleomagnetic poles between Eastern China and Indochina: a consequence of the extrusion of Indochina, Tectonophysics, 334, 101–113, 2001.

Yin, A. and Harrison, T. M.: Geologic evolution of the Himalayan-Tibetan Orogen, Ann. Rev. Earth Planet. Sci., 28, 211–280, 2000.

You, Y., Huber, M., Muller, R. D., Poulsen, C. J., and Ribbe, J.: Simulation of the Middle Miocene Climate Optimum, Geophys. Res. Lett., 36, L04702, doi:10.1029/2008GL036571, 2009.

Zachos, J., Pagani, M. N., Sloan, L., Thomas, E., and Billups, K.: Trends, rhythms, and aberrations in global climate 65 Ma to Present, Science, 292, 686–693, 2001.

Zanchi, A., Zanchetta, S., Garzanti, E., Balini, M., Berra, F., Mattei, M., and Muttoni, G.: The Cimmerian evolution of the Nakhlak–Anarak area, Central Iran, and its bearing for the reconstruction of the history of the Eurasian margin, Geol. Soc. Spec. Publ., 312, 261–286, 2009.

Zhu, B., Kidd, W. S. F., Rowley, D. B., Currie, B. S., and Shafique, N.: Age of initiation of the India-Asia collision in the East-Central Himalaya, J. Geol., 113, 265–285, 2005.

Table 1. APW paths used for paleogeographic reconstructions.

				NAM		SAM		AFR		EUR	
A1 (Ma)	A2 (Ma)	*N*	A95 (°)	Lat (° N)	Lon (° E)	Lat (° N)	Lon (° E)	Lat (° N)	Lon (° E)	Lat (° N)	Lon (° E)
10	8.3	54	2.0	85.0	168.1	85.9	151.0	85.3	173.5	85.4	162.5
20	18.9	38	2.7	83.3	164.2	84.7	133.8	83.9	175.9	84.0	154.8
30	29.5	23	3.8	81.5	169.2	83.7	132.6	81.8	190.7	82.8	158.1
40	40.0	24	3.2	79.5	174.4	82.6	139.2	79.0	201.1	81.3	162.4
50	52.2	31	3.4	77.9	179.3	82.1	141.8	76.9	210.3	80.9	164.4
60*	*	4	1.7	75.9	192.8	82.4	162.8	74.4	221.9	80.7	184.0
70*	*	4	1.7	75.9	192.8	83.2	157.7	74.2	224.4	81.0	182.5
80*	*	4	1.7	75.9	192.8	83.3	163.5	71.7	231.3	81.0	180.9
90*	*	4	1.7	75.9	192.8	84.8	161.1	68.2	239.5	80.8	179.7
100*	*	4	1.7	75.9	192.8	86.0	178.1	63.5	247.4	80.8	178.5
110*	*	4	1.7	75.9	192.8	87.9	217.6	59.8	254.9	80.6	178.9
120*	*	4	1.7	75.9	192.8	86.9	284.3	56.3	262.0	80.4	180.5

				IND		AUS		ANT	
A1 (Ma)	A2 (Ma)	*N*	A95 (°)	Lat (° N)	Lon (° E)	Lat (° N)	Lon (° E)	Lat (° N)	Lon (° E)
10	8.3	54	2.0	86.2	216.4	87.0	254.3	86.0	160.8
20	18.9	38	2.7	84.0	246.8	82.8	287.8	85.4	151.9
30	29.5	23	3.8	79.1	266.1	76.6	291.0	85.1	162.2
40	40.0	24	3.2	73.1	272.4	71.7	289.8	84.3	172.4
50	52.2	31	3.4	63.3	276.4	68.2	293.0	84.7	174.7
60*	*	4	1.7	52.5	277.1	65.1	292.9	84.6	203.5
70*	*	4	1.7	39.1	280.0	64.4	298.5	86.6	209.5
80*	*	4	1.7	31.6	282.1	62.5	302.0	87.6	243.4
90*	*	4	1.7	24.2	288.2	61.3	309.3	88.5	341.6
100*	*	4	1.7	16.3	293.6	59.3	316.1	85.5	11.7
110*	*	4	1.7	11.3	294.9	57.2	325.2	80.5	22.0
120*	*	4	1.7	6.2	298.4	54.3	335.0	74.5	26.8

Paleopoles from different continents (NAM, North America; SAM, South America; AFR, Africa; EUR, Eurasia; IND, India; AUS, Australia; ANT, East Antarctica) had been transferred to common (NAM) coordinates using rotation parameters from Besse and Courtillot (2002) and averaged in 20 Myr windows stepped every 10 Myr. The mean paleopoles of the composite APW path were then transferred from NAM coordinates to the different continents. Mean paleopoles for 10 to 50 Ma are from Besse and Courtillot (2003); mean paleopole for 60–120 Ma is the standstill superpole in NAM coordinates from Kent and Irving (2010). A1 is age of center of 20 Myr averaging window, A2 is mean age of poles in the 20 Myr window, *N* = number of paleomagnetic pole entries, Lat is latitude and Lon is longitude of mean paleomagnetic pole and A95 is its radius of circle of 95 % confidence. *Based on average of mean poles listed in Kent and Irving (2010; Table 6) for 60, 80, 100 and 120 Ma windows in NAM coordinates and propagated to other continents via interpolated Euler poles from Besse and Courtillot (2002).

Table 2. Total rotation poles for the SE Asian blocks.

Age	W. Sumatra			N. Indochina			S. Indochina-E. Sumatra-Java			C. Indochina-Borneo		
Ma	Lat	Lon	Ω	Lat	Lon	Ω	Lat	Lon	Ω	Lat	Lon	Ω
0	0.0	0.0	0.0	0.0	0.0	0.0	0.0	0.0	0.0	0.0	0.0	0.0
5	13.7	94.5	5.2	11.5	90.7	5.3	11.5	90.7	5.3	11.5	90.7	5.3
10	11.4	96.2	9.2	9.4	92.0	9.2	9.4	92.0	9.2	9.4	92.0	9.2
15	14.1	102.2	9.7	7.5	91.5	9.7	7.5	91.5	9.7	7.5	91.5	9.7
30	10.6	90.8	21.9	7.2	86.6	22.2	7.2	86.6	22.2	7.2	86.6	22.2
40	4.6	93.3	28.8	5.9	88.6	28.5	1.9	90.2	29.1	4.1	90.4	33.1
50	4.5	93.6	29.3	5.8	89.0	29.0	1.8	90.6	29.6	4.0	90.7	33.6
60	3.4	99.3	30.2	4.6	95.0	29.6	0.7	96.4	30.2	2.8	95.8	34.3
70	3.5	99.0	29.9	4.7	94.5	29.3	0.8	96.0	30.0	2.9	95.4	34.0
80	3.6	98.5	29.8	4.8	94.1	29.3	0.9	95.5	30.0	3.0	95.0	34.0
90	3.6	98.1	30.0	4.9	93.7	29.5	1.0	95.1	30.2	3.1	94.7	34.2
100	3.7	97.7	30.0	4.9	93.3	29.5	1.0	94.7	30.1	3.1	94.3	34.2
110	3.7	97.8	30.2	4.9	93.4	29.7	1.0	94.8	30.4	3.1	94.4	34.3
120	3.6	98.2	30.4	4.8	93.8	29.9	0.9	95.3	30.6	3.0	94.8	34.6

Rotation poles (Lat = latitude ° N, Lon = longitude ° E, Ω = rotation angle, positive counterclockwise) obtained by multiplying the paleomagnetic Euler poles of Eurasia (derived from Table 1) with the step-by-step Euler poles of the SE Asian blocks relative to Siberia (Eurasia) accumulated in the 0–40 Ma time window (derived from Replumaz and Tapponnier, 2003). For the previous 50–120 Ma interval, the SE Asia blocks are considered tectonically coherent and moved with Siberia (Eurasia). N = North, S = South, E = East, W = West, C = Central.

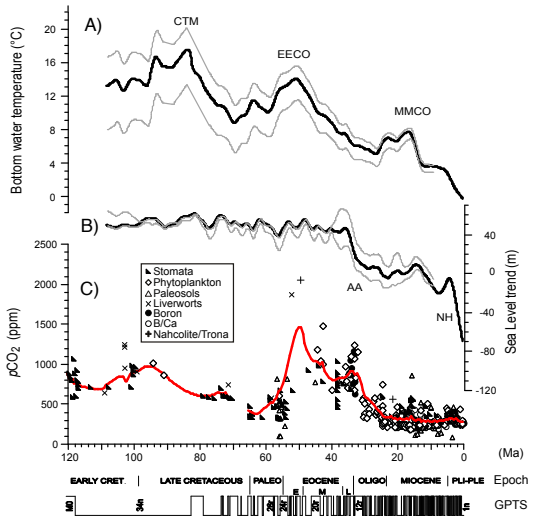

Fig. 1. Bottom water temperatures **(A)** and reconstructed sea levels **(B)** since the Early Cretaceous (Cramer et al., 2011) smoothed to emphasize variations on > 5 Myr timescales. CTM is Cretaceous thermal maximum, EECO is Early Eocene climatic optimum, and MMCO is Middle Miocene climatic optimum; AA is sea-level drop at the inception of Antarctic ice sheets, and NH is sea-level drop at the inception of Northern Hemisphere ice sheets. **(C)** Atmospheric pCO_2 estimates from various proxies from compilation of Royer (2010) for pre-70 Ma interval (except paleosol estimates, which are highly scattered and have not been plotted) and of Beerling and Royer (2011) for post-70 Ma interval. Simple smoothing functions have been fit (heavy curved line) through the mean pCO_2 estimates provided in the compilations. Ages according to GPTS (geomagnetic polarity time scale) of Cande and Kent (1995). Geologic epochs are Early Cretaceous, Late Cretaceous, Paleocene, Eocene (E for Early, M for Middle, L for Late), Oligocene, Miocene, and Pliocene and Pleistocene.

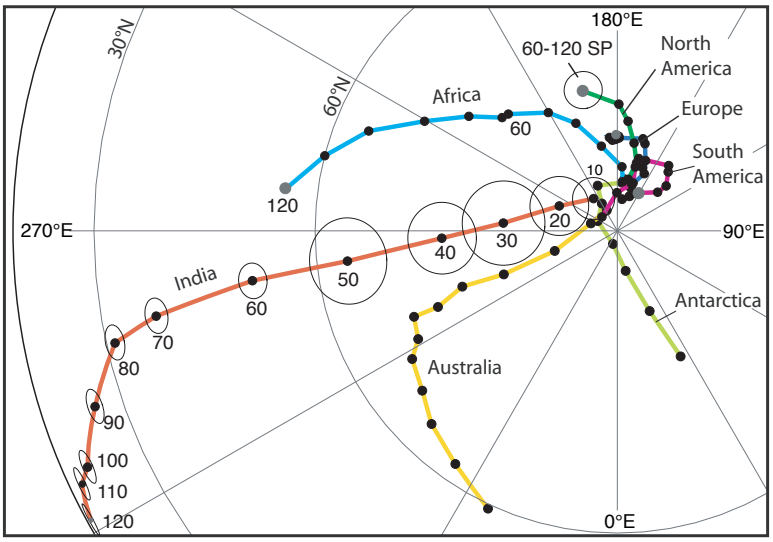

Fig. 2. Apparent polar wander paths for Africa, Antarctica, Australia, Eurasia, India, North America and South America based on a composite APWP using paleopoles from all the main continents that were brought to common coordinates using finite rotation poles used by Besse and Courtillot (2002), averaged with a sliding 20 Myr window every 10 Myr, and the mean poles transferred back to the different continents; hence the differences in APWP for the various continents reflect relative motions according to the finite rotation poles used for the plate reconstructions. Mean paleopoles for 10 to 50 Ma are from Besse and Courtillot (2002, 2003); mean paleopole for 60 to 120 Ma is an average of global igneous data (superpole labeled 60–120 Ma SP with 95 % confidence circle and based on 60, 80, 100 and 120 Ma mean poles from Kent and Irving (2010) for a standstill in apparent polar wander in North American coordinates (Table 1). Circles of 95 % confidence that are shown on the India APWP are in common for the APWP projected to other continents.

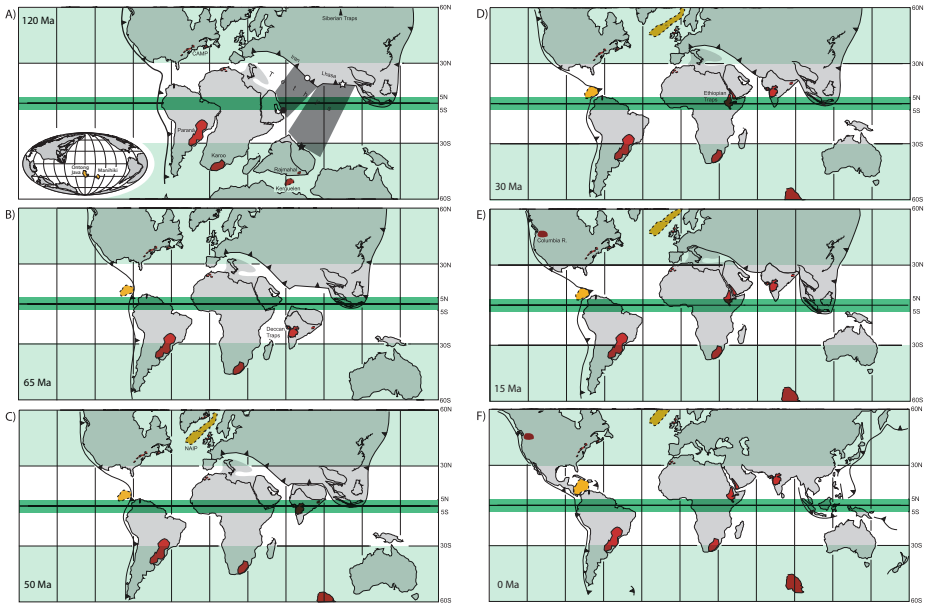

Fig. 3. Paleogeographic reconstructions based on a composite APWP (Table 1, Fig. 2), the finite rotation poles given by Besse and Courtillot (2002) from Muller and Roest (1992), Muller et al. (1993), and Srivastava and Tapscott (1986) for the major continents and the rotation poles of Replumaz and Tapponnier (2003) for SE Asia blocks, as discussed in text. **(A)** 120 Ma at about Magnetic Anomaly M0; **(B)** 65 Ma at about Anomaly 29; **(C)** 50 Ma at about Anomaly 21; **(D)** 30 Ma at about Anomaly 11; **(E)** 15 Ma at about Anomaly 5 B; **(F)** present-day geography. The equatorial humid belt ($P > E$: precipitation > evaporation) between 5° S and 5° N is represented by darker green shading, the temperate humid belts ($P > E$) from 30° to beyond the latitudinal limits (60°) of our paleogeographic reconstructions are represented by lighter green shading, with the intervening arid belts ($P < E$) unshaded, all based on general circulation climate model with idealized geography by Manabe and Bryan (1985). Large continental basaltic provinces are shown in red, large submarine provinces in orange. Paleogeographic maps were made with PaleoMac software (Cogné, 2003).

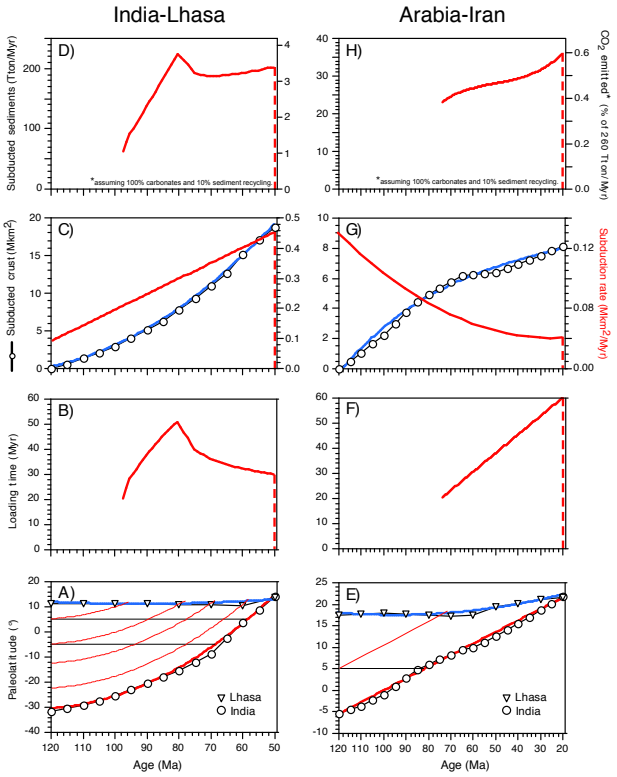

Fig. 4. Caption on next page.

Fig. 4. Estimates of decarbonation in Tethyan subduction factory. Panels **(A)**–**(D)** refer to the subduction of Tethyan crust between Greater India and Lhasa (Asia). **(A)** Paleolatitude curves for Northern Greater India (filled star in Fig. 3a) and Southern Lhasa block (unfilled star in Fig. 3a) with 2nd order polynomial fits used to calculate the subduction time and the loading time of oceanic crust during passage through hypothesized equatorial upwelling belt (5° S–5° N). **(B)** Sediment loading time for passage through equatorial upwelling belt (5° S–5° N) of oceanic crust subducted under Asia. Curve starts at 97 Ma with a nominal 20 Myr loading time because the oceanic crust was sitting in the equatorial belt since appearance of pelagic carbonates and well before onset of subduction. **(C)** Amount of Tethyan crust as function of time between northern Greater India and southern Lhasa block that was eventually subducted under Asia plotted with a 2nd order polynomial fit resampled every 1 Myr (blue line) and red curve showing subduction rate (scale on right) as 1st derivative of the polynomial subduction curve. **(D)** Amount of equatorial bulge sediments on Tethyan crust subducted under Asia per Myr as a function of time. The axis on the right is the CO_2 emitted by these sediments expressed as percentage of modern outgassing rate of 260 Tton Myr^{-1}, assuming the sediments were 100 % carbonates and 10 % recycled. Panels **(E)**–**(H)** refer to the subduction of Tethyan crust between Arabia and Iran (Asia) following the same procedure illustrated for India-Lhasa in panels **(A)**–**(D)**, with the only notable differences that the time scale extends to 20 Ma and the paleolatitude curves (in **E**) are for the southeastern margin of Arabia (filled circle in Fig. 3a) and the western margin of the Iran block (unfilled circle in Fig. 3a).

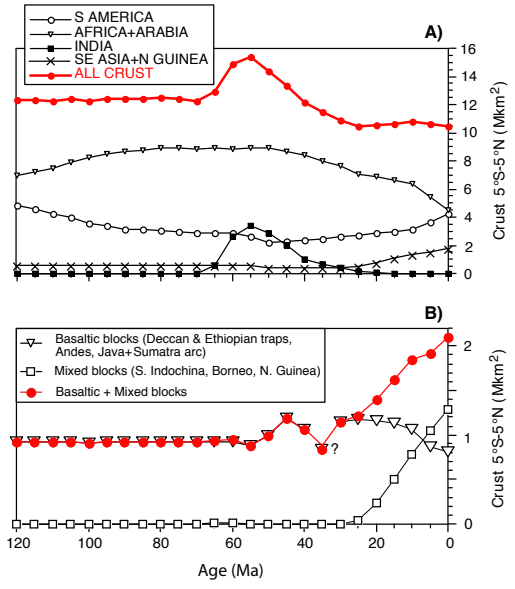

Fig. 5. (A) Estimates of land area within equatorial humid belt (5° S–5° N) as a function of time since 120 Ma obtained by applying the composite APWP (Table 1; Fig. 2) and finite rotation poles of Besse and Courtillot (2002) for major continental blocks and the rotation poles of Replumaz and Tapponnier (2003) for SE Asia blocks as discussed in text. **(B)** Estimates of key (most weatherable in the most favorable environment) land areas comprised of volcanic arc provinces (Java, Sumatra, Andes), large basaltic provinces (Deccan Traps, Ethiopian Traps), and mixed igneous-metamorphic provinces (South Indochina, Borneo, New Guinea) in the equatorial humid belt (5° S–5° N) as a function of time from 120 Ma to Present. The rest of the world's continental regions in the equatorial humid belt are generally characterized by low elevation (Amazon and Congo Basins), hence weathering tends to be low and transport-limited.

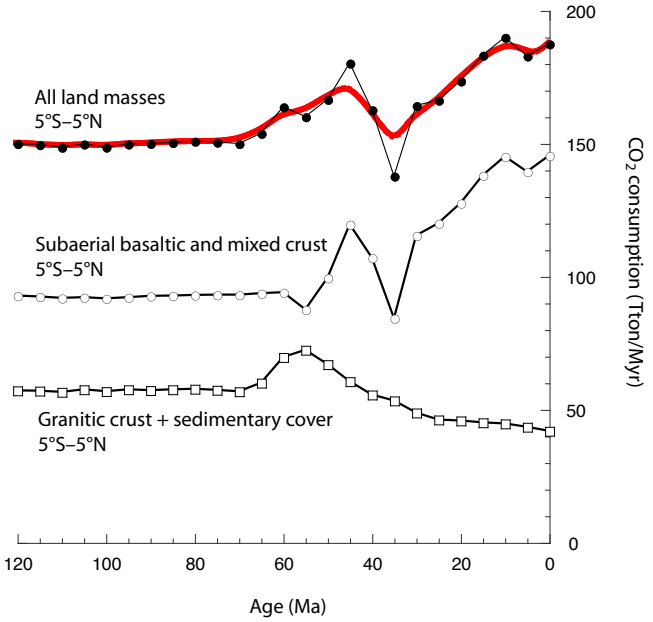

Fig. 6. CO_2 consumption rates from silicate weathering since 120 Ma of land areas in equatorial humid belt (5° S–5° N) obtained by multiplying a nominal CO_2 consumption rate of 100 Mton CO_2 Myr^{-1} km^{-2} for basaltic provinces and 50 Mton Myr^{-1} km^{-2} for mixed basaltic-metamorphic provinces (Dessert et al., 2003) and an order of magnitude less (5 Mton Myr^{-1} km^{-2}) for the remaining continental land areas (Gaillardet et al., 1999) to the corresponding cumulative distribution curves in Fig. 5. For reference, the consumption of 1 Tton CO_2 Myr^{-1} can be sustained by introducing into the equatorial humid belt or rejuvenating roughly 10 000 km^2 of the SE Asia arc terrane every million years.

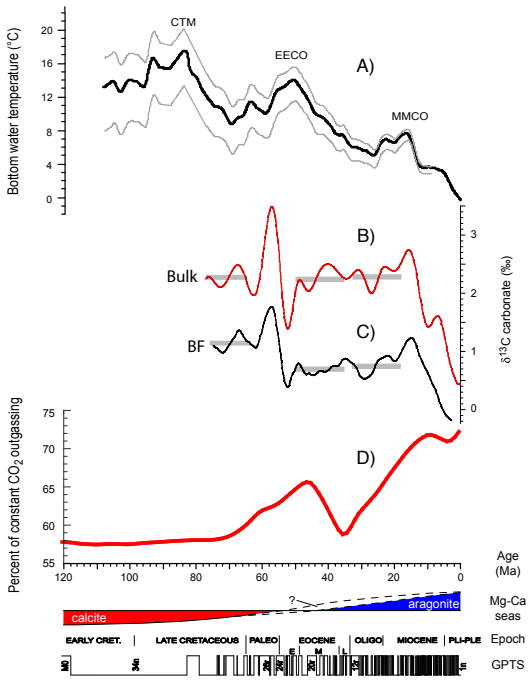

Fig. 7. **(A)** Bottom water temperatures (Cramer et al., 2011; see caption to Fig. 1 for explanation); **(B)** $\delta^{13}C$ carbonate data from whole sediment (Bulk) (smoothed SSA curve from Katz et al., 2005) and **(C)** $\delta^{13}C$ carbonate data from benthic foraminifera (BF) from the Pacific (smoothed trend from Cramer et al., 2009), with mean values over selected intervals (77–65 Ma, 50–35 Ma, 33–18 Ma) shown by gray bars; **(D)** secular change in CO_2 consumption rate from silicate weathering of all land masses in equatorial humid belt (5° S–5° N) (smoothed curve from Fig. 6) expressed as percentage of modern volcanic outgassing rate of 260 Tton Myr^{-1} (Gerlach, 2011; Marty and Tolstikhin, 1998). Ages based on GPTS of Cande and Kent (1995). Below age axis is diagrammatic representation of oscillation between Mg-poor calcite seas and Mg-rich aragonite seas (Sandberg, 1983).